D5.3 - Test-bench campaign

DATE: February 2018

PROJECT COORDINATOR:

WavEC Offshore Renewables

GRANT AGREEMENT NR: 641334

The WETFEET – Wave Energy Transition to Future by Evolution of Engineering and Technology project has received funding from the European Union's Horizon 2020 programme under grant agreement No 641334.

Project	WETFEET – Wave Energy Transition to Future by Evolution of Engineering and Technology		
WP No.	5	WP Title	Submerged Polymeric PTO Breakthrough
Deliverable No.		5.3	
Nature (R: *Report*, P: *Prototype*, O: *Other*)		R	
Dissemination level (PU, PP, RE, CO)		PU	
Lead beneficiary:		SELMAR	
Contributing partners		SELMAR, UNITN	
Authors List:		Marco Fontana, Francesco Biral, Luca Zaccarian, Daniele Bortoluzzi, Caludio Salomon, Claudio Raggi, Andrea Gussoni.	
Quality reviewer		Reinhard Schwoediauer	
Status (F: final; D: draft; RD: revised draft):		F	
Due Delivery Date:		30 December 2017	
Actual Delivery Date:		06 April 2018	

Version no.	Dates and comments
1	3 Nov 2017, definition of the preliminary structure of the report
2	30 Nov 2017, contributes on the setup design
3	20 Dic 2017, contribution on test results
4	08 Jan 2018, final structure
5	08 Mar 2018, Final version including test elaboration
6	06 April 2018, Final Version, after internal review

Table of Contents

Table of figures

Table of tables

Executive summary

This report is the Deliverable 5.3 of the WETFEET H2020 project. The document reports on the main activities conducted in the framework of work package 5 (WP5), and more specifically focussed on the task 5.3 “Manufacturing and test-bench of polymeric PTO”.

The main aims of WP5 are: (1) the study and development of a sensing/control system for a PTO for WECs based on Dielectric Elastomer Generators (DEGs) including a preliminary prototype of a power electronics; (2) the study of effective controllers for the DEG-PTO and (3) the design and development of a laboratory test-bench to perform Hardware In the Loop (HIL) simulations.

DEGs are elastomeric electrostatic transducers that are able to directly convert the mechanical energy that is required to induce a deformation of their shape into Direct Current (DC) electrical energy. Preliminary studies of the application of these devices in the wave energy sector have been conducted in the framework of the European Commission funded (FP7) project PolyWEC (www.polywec.org). In such a project, the feasibility of the implementation of WECs based on DEG-PTO has been demonstrated through a set of small scale prototypes that have been tested in laboratory and wave-tank facilities. Such early works are characterized by the following limitations:

- The DEG prototype was built in acrylic rubber which is suitable for demonstration purposes but not sufficiently reliable and performant to be envisaged for advanced/large-scale implementations;
- The DEG prototype featured carbon grease electrodes which are suitable for demonstration purposes but totally unsuitable for applications in real environment;
- The DEG PTO electronics was suitable for demonstration purpose but presented several limitations in terms of controllability of the devices and efficiency;
- A single control strategy has been studied and tested; this was based on a simple sub-optimal strategy limited to indirect measures of air pressure.

The activities that are reported in this document are developed in this framework to advance the current status of development of such basic components of DEG-PTOs.

Specifically, the work was focused on the following main aspects:

- Manufacturing study of a solid-state reliable PDMS based DEG membrane;
- Study of a power electronics that is required for the control of the DEG-PTO in operational conditions;
- Implementation of a small-scale prototype (in the range of 3-10 W), the sensing equipment, and the power electronics to be integrated in a HIL setup for the laboratory test of a fully functional DEG, i.e. a DEG that is actually able to efficiently convert mechanical oscillating energy into electricity;
- Study, in simulation environment, of the control strategies that should adopted in order to maximize the performance of the developed power and sensing systems.

This document is organized as follows.

In the first part of the document a brief introduction to the DEG-PTO technology is provided. The following Section 2 illustrates the HIL setup that has been purposely built to make it possible to test different DEG-PTOs in operational conditions. Such a setup is based on a computer-controlled linear pneumatic driver which is able to inflate and deflate the DEG membrane prototype according to suitable hydrodynamic real-time simulations.

Section 3 describes the work done to identify a suitable manufacturing procedure for the DEG membrane. Specifically, a PDMS multilayer DEG membrane has been manufactured and integrated. Section 4 describes the tests campaign that has been conducted on the developed DEG-PTO prototype. Lastly, Section 5 draws some conclusions on the developed work and on future perspectives for the development of DEG technology within the wave energy sector.

LIST OF ACCRONYMS

CD-DEG	Circular Diaphragm Dielectric Elastomer Generator
DC	Direct Current
DE	Dielectric Elastomers
DEG	Dielectric Elastomer Generator (to refer to the whole generator)
DOF	Degree of Freedom
ECU	Elastomeric Conversion Unit (to refer to the sole DE membrane and conductive electrodes)
DAB	Dual Active Bridge
HIL	Hardware In the Loop
HV	High Voltage
ICD-DEG	Inflated Circular Diaphragm Dielectric Elastomer Generator
LCOE	Levelized Cost of Electricity
NS	Negative Spring
OPEX	Operational Expenditures
OWC	Oscillating Water Column
PD	Pressure Differential
PTO	Power Take-Off
SPC	Sensing, Power and Control
TRL	Technology Readiness Level
TPL	Technology Performance Level
WEC	Wave Energy Converter
WP	Work Package

1. Introduction

Dielectric elastomer control

This section illustrates an introduction to working principle of WECs based on Dielectric Elastomer Generators (DEGs), providing a context of the technology status from the point of view of the techniques for construction/manufacturing and operation/control strategies and electronics In this framework, we provide a context of the work that is developed within the WETFEET project with respect to the state of the art.

1.1. Working principle and control

The search and development of adequate control algorithms for WECs based on DEGs have to be carried out using dynamic modelling tool since generally there is a strong interaction between the DEG-PTO and the WEC hydrodynamics. Specifically, in WECs based on more conventional PTO, the presence of the PTO does not affect the overall stiffness of system; thus, the controller can be synthetized just to make the PTO provide an appropriate damping to the primary mover. This approach cannot be pursued with DEG-PTOs that, due to their nature, provide a significant contribution to the stiffness in the dynamic response of the WEC, with the value of such a stiffness depending on the level of electrical activation.

For example, let us consider a series of incoming waves toward a generic DEG-based WEC device. In this system, the deformation of the DEG is influenced by the water motion but the amplitude of water motion is in turn affected by the deformation of the DEG. This means that when the DEG extracts energy, both the dynamics influence each other (that is, they are fully coupled). In this case, since electrical activation modifies the stiffness characteristic of the DEG (thus the overall system natural frequency), control operation could also contribute to the overall dynamics of the system. Thus, in order to synthetize and develop appropriate controllers, it is necessary to build an integrated model of the system that takes into account the hydrodynamics, the elastic and electrical response of the DEG. This model has to include also the dynamic response of the power control electronics.

In previous work of some of partners involved in WP5, the generic control problem of a DEG-WEC has been theoretically considered for the architecture of the Oscillating Water Column (OWC) WEC equipped with the Inflated Circular Diaphragm Dielectric Elastomer Generator (ICD-DEG) [1]. Such analysis considers an optimization approach that is based on validated models, however the conceived algorithms have not been tested on a real prototype. Actually, previous experimental works [2][3][4] consider only demonstration prototypes that were developed for the validation of concepts but did not include all the essential features that are necessary to provide an effective test on the system controllers.

Differently, in the activities of WP5 of WETFEET project, one of the final aim is the development of a setup that enables the experimental testing of a scaled DEG-PTO in fully functional operation i.e. equipped with the following new features:

- fully functional sensing and power electronics;
- real-time hardware in the loop controllers and hydrodynamic models that are suitable to represent also the submerged case;
- possibility of evaluating the global efficiency of the system;
- high quality DEG-PTO prototype fabricated according to a repeatable and reliable procedure;

In the following section a brief description of the generation cycle of a generic DEG is presented in order to explain the basic working principle and define the generic functionalities that are required to the sensing and control electronics to be able to perform such cycles.

1.1.1. DEG generation cycle

With reference to the control law, and based on the aforementioned operational constraints, we now recall the principal ways to extract energy from DEGs.

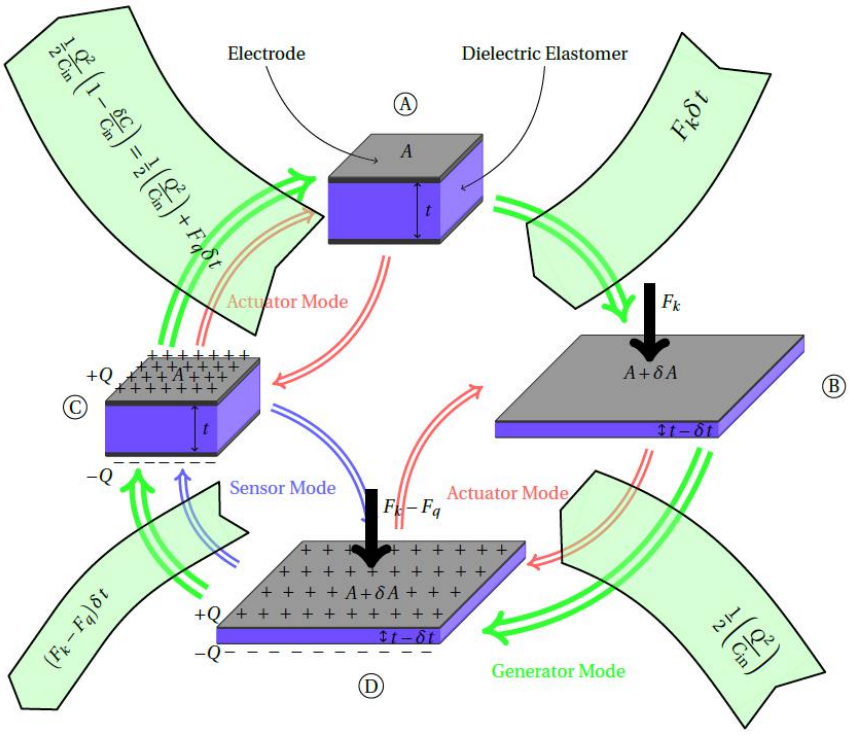

FIGURE 1-1 DIELECTRIC ELASTOMER WORKING PRINCIPLE. THE RED ARROWS INDICATE HOW THE DE WORKS AS ACTUATOR; THE BLUE ARROWS SHOW HOW IT WORKS AS A SENSOR AND THE GREEN ARROWS DENOTE HOW IT WORKS AS GENERATOR, CONSIDERING A CYCLE WITH A CONSTANT CHARGE.

The basic phases and concepts of DEG working principle are reported in Figure 1-1, where Q represents the amount of charge on the electrodes, C represents the capacitance of the DEG (C_{in} being the capacitance of the membrane in the deformed state), F_k is the compressive force applied on the DEG surface and F_q is the electric force due to the charge.

Considering the electrostatic potential energy stored in the DE electric field, U_{le}, and the electric work performed on the DEG by the external circuit, W_{el}, the infinitesimal energy extracted by the DEG in correspondence to an infinitesimal deformation is

$$dW_{DEG} = dU_{le} - dW_{el} \tag{1}$$

where dU_{le} and dW_{el} can be obtained from an energy balance equation that reads as follows:

$$\mathrm{dW}_{DEG} = \frac{V^2}{2}\mathrm{d}C + VC\mathrm{d}V - V^2\mathrm{d}C + VC\mathrm{d}V = -\frac{1}{2}V^2\mathrm{d}C, \tag{2}$$

where $\mathrm{d}V$ and $\mathrm{d}C$ represent the generic infinitesimal variations of voltage V and capacitance C, respectively. From equation (1.2), it can be seen that electricity is positively generated when $\mathrm{d}C < 0$. That is, the DEG behaves as a generator (producing a positive electrical energy output) if it is electrically activated while its capacitance decreases. Therefore, to harvest energy out of the deformation of the DEG, the voltage across the DE electrodes needs to be properly regulated.

Referring to the *Q*-*V* plane, a generic control pattern followed by the generator in a cycle is represented by any closed curve included within the physically allowable operating space. The area enclosed by the considered curve is numerically proportional to the mechanical energy converted into electrical energy in that cycle, which is given by

$$W_{DEG} = \int \mathrm{d}W_{DEG} = -\int V\mathrm{d}Q \tag{3}$$

In particular, the limiting curves define a cycle, which encloses an area equal to the maximum energy that can be converted in a single cycle by the DEG (see Figure 1-2). With reference to this figure, the generation cycle is controlled as follows. In State 1 the DEG is kept inactive during its expansion, i.e. the capacitance increases. This part of the cycle is not visible in the Q-V plane because it collapses in the axes origin. In state 2, the control is activated when the membrane reaches the maximum deformation. This phase is identified by red arrows (from O→E). The control law is followed in order to obtain the chosen strategy. This phase is identified by blue arrows from E→F. The DEG is discharged when the capacitance is minimum, that is, when the ICD-DEG is flat. This phase is identified by black arrows from F→O. The different control strategy features the following attributes:

- **Constant Charge** (see Figure 1-2-a). This control scheme is based on putting a fixed amount of charge on the electrodes when the capacitance is maximum and then extracting the same amount of charge at a higher voltage. This control strategy is very simple to implement, but the amount of energy that can be extracted with respect to the feasible physical region is poor. Some experimental results using this kind of control scheme were reported in [2].
- **Constant Voltage** (see Figure 1-2-b). In order to implement this control strategy, it is necessary to connect a battery to the electrodes when the capacitance decreases. This control scheme is easy to implement, but requires choosing an appropriate voltage depending on the stretch in order to reach high energy extraction levels.
- **Electric Field Control** (see Figure 1-2-c). This control strategy tries to maximise the energy harvested in the cycle. The scheme consists in choosing the right voltage to be imposed between the electrodes as:

$$\bar{V}(\lambda) = \bar{E}t(\lambda) = \beta E_{BD}t(\lambda) \tag{4}$$

where t is the thickness of the membrane (in the current deformed configuration), $\bar{E}$ is the electric field applied on the DEG and β is a safety factor. This strategy requires the knowledge of the thickness value in order to obtain the right voltage to be impose between the electrodes. This information can be obtained by using other information, such as the DEG tip elevation or its capacitance value.

- **Feasible physical region.** This control scheme maximises the energy harvested in the cycle. It is based on the following law

$$V(\lambda) = \beta \min(V_{\sigma_0}(\lambda), V_{E_{BD}}(\lambda)) \tag{5}$$

where $V_{\sigma_0}(\lambda)$ is a function that returns the exact value of voltage that verifies the buckling and $V_{E_{BD}}(\lambda)$ is a function that returns the exact value of voltage that verifies the breakdown condition of the membrane. Both functions require the knowledge of the actual value of stretch, λ, of the DEG. For this reason, execution of this control scheme is very difficult unless a reliable model of the DEG is available.

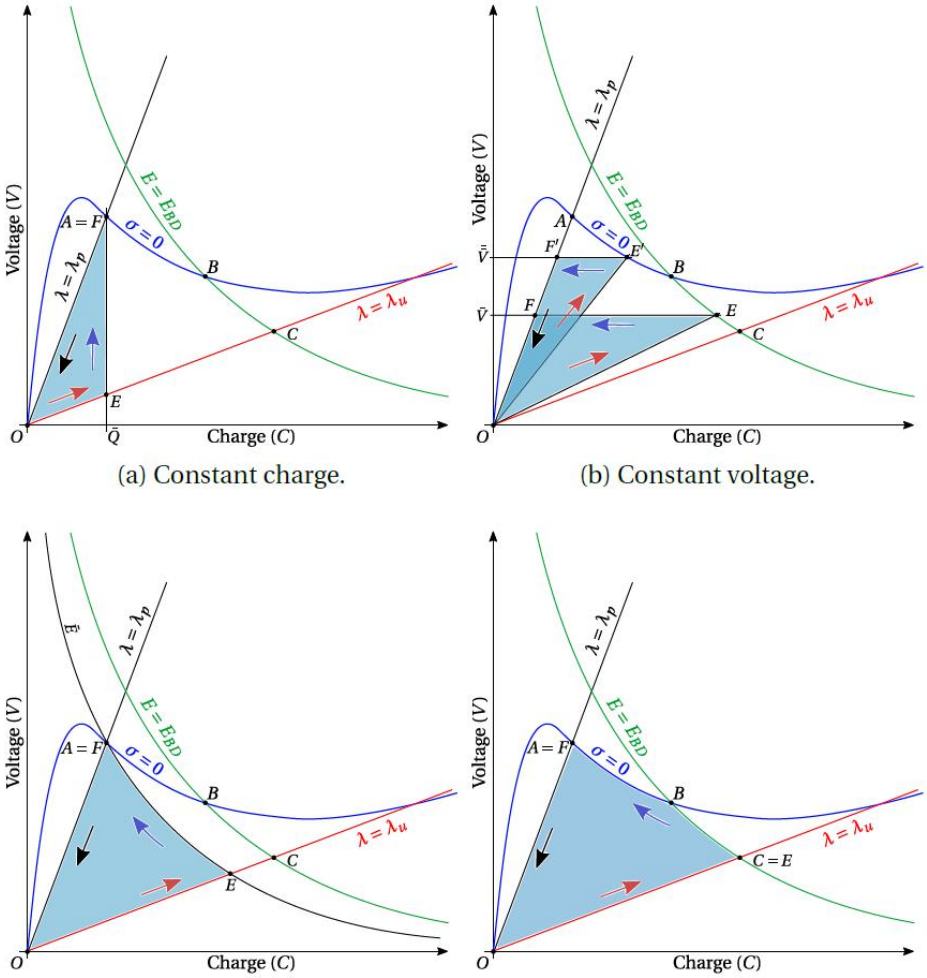

FIGURE 1-2 Q-V PLOTS OF THE BASIC GENERATION CYCLES:

All the control strategies presented here are based on a specific path in the *Q-V* plane. However, all of them use the concept of a basic four phase control scheme with the following main steps:

1. The DEG is kept inactive during its expansion, when the capacitance increases. This part of the cycle is not visible in the *Q-V* plane because it collapses in the plane's origin. This phase is called "inactive phase".

2. When the membrane reaches its maximum deformation, the control is activated. In Figure 1-2, this phase is identified by the red arrows (from O→E). This phase is called the "charging phase".
3. The control law is followed in order to obtain the chosen strategy. This phase is identified by the blue arrows from E→F. This phase is called "harvesting phase" or "active phase".
4. The DEG is discharged when the capacitance is minimal (namely, when the DEG is flat). This phase is identified by the black arrows from F→O. This phase is called "discharging phase".

More generally, voltage and charge of the DEG can be controlled according to closed loops in the *Q-V* plane, having each cycle corresponding to an amount of energy converted that is proportional to the enclosed area.

1.1.2. Definition of Functionalities of Sensing, Power and Control Electronics

On the basis of the previous description of the ideal generation cycles of a DEG, we can define the basic functionalities that are required to the sensing, power and control (SPC) system to be able to automatically operate.

Specifically, these are the basic functionalities that should be implemented during the cyclical operation:

(1) *Measure and elaborate* the status of deformation (or capacitance, since they are related to each other) of the DEG in order to instantaneously decide the charging status of the device. This can be achieved in different ways. An indirect method was proposed and tested in previous studies on DEGs that are based on the ICD-DEG architecture. For these devices the electrical activation of the DEG can be easily decided on the basis of the measure of the pressure and the calculation of its derivative. In the case of submerged DEG, the issue can be solved through the technique of the self-sensing that is implemented and described in the following sections of this document.

(2) *Bidirectional charging-discharging:* the flux of charge on the DEG needs to be bidirectional since the loops in the *Q-V* plane must be closed. This functionality has not been implemented previously with effective solutions. In previous studies, the employed electronics was developed for the purpose of demonstration and the contribution of its poor efficiency on the global performances of the DEG-WEC was ignored (i.e., performance analysis was restricted to the consideration of the amount of electrical energy generated by the DEG, regardless of the successive dissipation in the conditioning circuit). In this document, we describe the study and the implementation of a high efficiency electronics that is potentially able to implement energy cycles with efficiency in the order of 90-95 %.

2. Testing setup

One of the main objectives of the activities conducted in WP 5 of the WETFEET project is the development and the experimental short-term laboratory testing of a small-scale physical model to validate and optimise system functionality, behaviour and performance. Results of these activities are going to be used to identify and correct unforeseen design and performance issues at an early stage, build confidence and inform the next stages of testing.

Specifically, the aim is to develop a fully functional DEG-PTO system that includes: Elastomeric Conversion Unit (ECU), power electronics, and controller with required sensors. Aiming in the future at a full-scale single system with power output in the range of 100 kW to 400 kW, the scaled DEG-PTO that is developed and experimentally investigated in this WP will have a scale in the range of 1:15 to 1:25 and a power output in the range of 1.5 W to 10 W.

The complete scaled DEG-PTO is mounted in a purposely developed HIL set-up that makes it possible its testing, with its controllers, in emulated OWC and PD WECs subjected to realistic sea wave conditions. The major objectives of these tests are: 1) characterization of the static and dynamic response of the DEG-PTO; 2) assessment of system maximal control force capability and energy conversion efficiency across the entire load regime; 3) characterization and demonstration of system survivability in extreme wave conditions.

A hardware-in-the-loop (HIL) setup that is needed for such kind of tests set-up has been purposely designed and has been built.

The final setup is shown in Figure 2-1 and it comprises:

- a DEG-PTO, equipped with the primary elastomeric conversion unit but also with sensors for measuring current and voltage, and other relevant variables for DEG-PTO operation and evaluation (for instance, pressure sensors, voltage probes);
- a custom hardware made of an upper cylindrical chamber open to ambient air pressure and a lower closed cylindrical air chamber with variable geometry regulated by means of an actuated piston (for instance using an electro-cylinder);
- HIL set-up control software and power electronics that implements real-time hydrodynamics models of specific WEC architectures and command the activation status of the ECU simulating the controller of the system.
- A commercial real-time target computer with I/O modules (such as a Speedgoat performance real-time target machine) is employed as the control hardware for both the HIL set-up and the DEG-PTO.

A preliminary report on the design of this HIL setup is provided in D5.2 while in this report we illustrate the final hardware system that has been assembled and tested in a campaign of experiments that make use of different prototypes of conversion units (manufactured according the procedure described in Section 3 of this document).

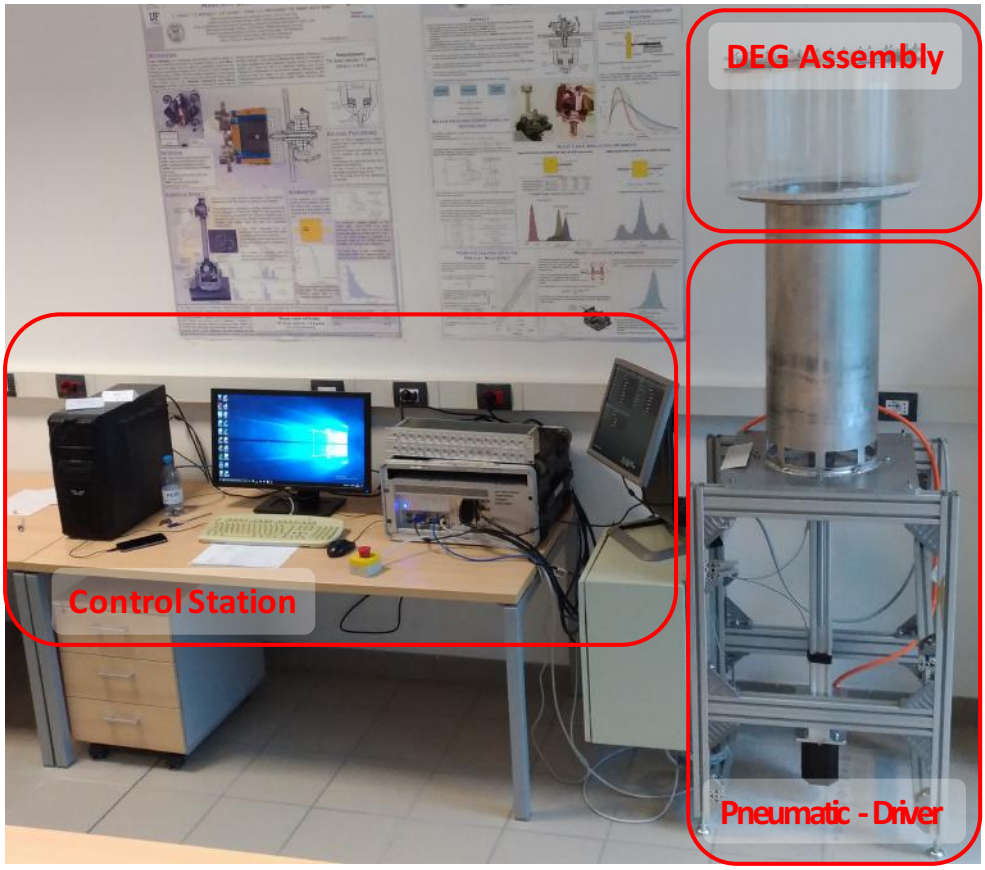

FIGURE 2-1: PICTURE OF THE WHOLE HIL SYSTEM COMPOSED BY CONTROL STATION, PNEUMATIC-DRIVER AND DEG-ASSEMBLY

2.1. Mechanical design and prototype

2.1.1. Design

The target pneumatic driver system has to be able to induce appropriate mechanical loading of the membrane in order to induce a variation in the capacitance of the DEG as illustrated in the previous section. The volume displaced per cycle is given by simple geometrical relations that take into account the variation of volume of the (quasi) spherical cap in the inflated condition.

Specifically,

$$V_c = 2\,V_s \approx \frac{4}{3}\pi R_s^3 \qquad (6)$$

Where V_c is the required volume displacement per cycle, V_s is the volume of the emispherical cap when fully inflated, and R_s is the radius of the ECU membrane.

The required pressure loads required to fully deform the ECU membrane is calculated by appropriately scaling of previous experimental results obtained on a smaller scale setup (with a membrane diameter of 0.13 m).

In the case of a 0.13 m membrane with a thickness of 0.2 mm, the maximum pressure required for reaching a fully deformed configuration - target deformation is achieved when the displacement of tip of the membrane is equal to the radius - was roughly 5 kPa.

In the setup that is designed in this project the target membrane radius is in the range of 0.15-0.25 m so results obtained for the 0.13 m membrane have to be scaled. If the geometry of the membrane is scaled up geometrically, i.e. thickness is increased of the same proportion of the radius, the pressure that is needed for the deformation remains constant and the power of the device assumes the values represented in Figure 2-2.

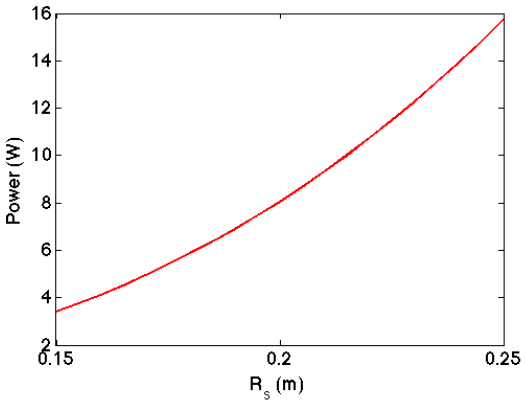

FIGURE 2-2 ESTIMATED POWER VS RADIUS OF THE MEMBRANE (LINEAR GEOMETRICAL SCALING) OUTPUT

In order to implement such required performances, the rational choice brings to consider a system that implements the linear displacement of the piston through the combination of a rotational motor and a linear stage.

The choice of appropriate combination of motor/driver and linear guide has been conducted with a certain level of safety margin which takes into account possible detrimental contributes of friction of the piston seals. The components that were chosen are the following:

Motor: Low Inertia Brushless, Kollmorgen AKM52L, power of 2.3 kW, nominal speed of 3500 rpm;

Driver: Kollmorgen AKD-P01206, power of 4 kW, EtherCAT communication, with on board position controller;

Linear stage: Festo, ball-guide with a maximum linear force of 4500 N and maximum speed of 1.2 m/s.

The chosen performances of these components make it possible to meet the requirements of force, speed and power with very large safety factor. This choice is done to introduce flexibility in the design options for the ECU membrane and in view of the possible implementation of larger scale/power systems.

The design of the mechanical assembly is represented in Figure 2-3. The motor has been placed at the bottom of the setup aligned with the linear stage. The output of the linear stage is connected to a piston that moves in an air cylinder inducing the air to flow forward and backward in a duct. The duct is U-shaped in order to guarantee easy access to the output flange where the DEG is attached. The top part of the air cylinder, holding the DEG, is made of plexiglass.

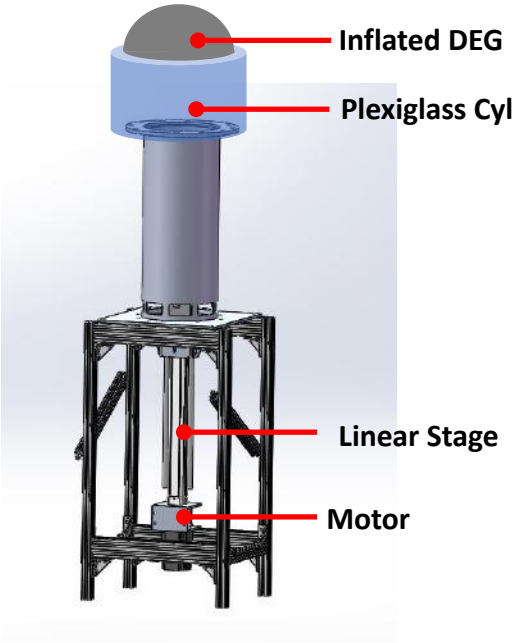

FIGURE 2-3 FINAL LAYOUT OF THE HARDWARE-IN-THE-LOOP WITH VERTICAL PISTON

2.1.2. Prototype implementation

The described prototype has been manufactured and assembled (see Figure 2-4). The main custom components feature the following characteristics:

- Cylinder: Bored to a diameter of D_{in}=300 mm and length of 600mm;
- Piston: white Delrin® made, weight 3.2 kg;
- Sealing: Polyurethane Sealpure 93
- DEG-holder: polycarbonate made with diameter D_h=0.5 m;
- Driver box: custom made driver box including:
    - Kollmorgen AKD-P01206, power of 4 kW, EtherCAT communication, with on board position controller
    - Power supplies and cabling;
    - Status monitoring lights;

Motion performances (tested):

- Maximum speed: 1.0 m/s;
- Maximum Pressure: P_{max}=0.5 bar (3.5 kN on the linear stage);
- Position accuracy: p=0.2 mm;
- Friction: static F_{fs}=100-120 N; dynamic F= F_{fs}=60-80 N;

Figure 2-4 shows the main components of the mechanical assembly including cylinder, piston, DEG-holder and main electronic components.

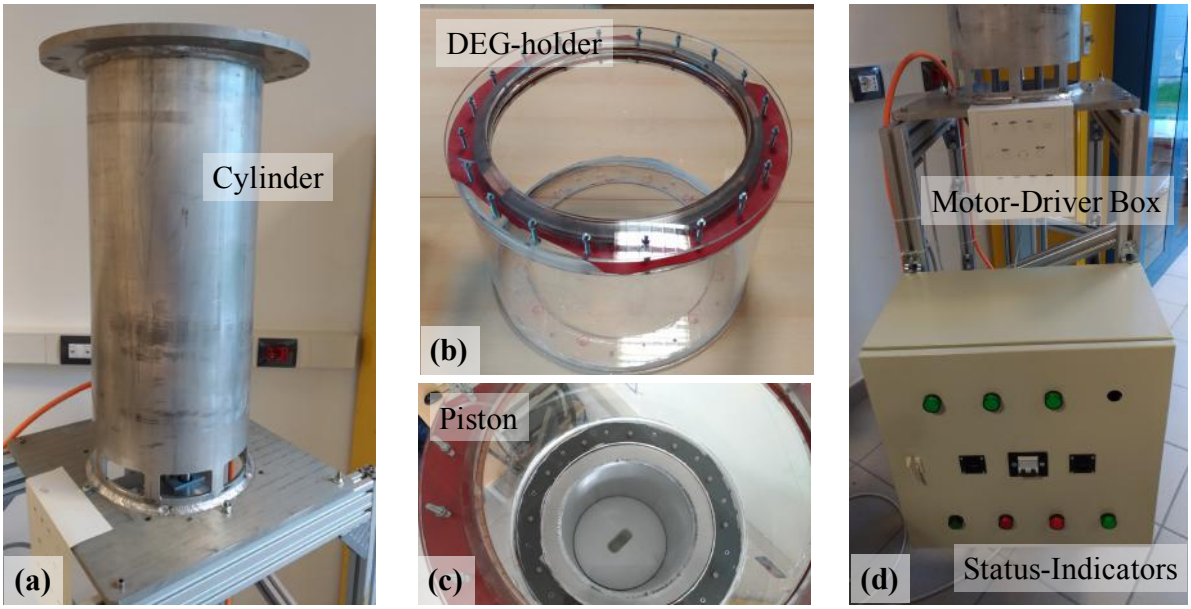

FIGURE 2-4 MAIN MECHANICAL COMPONENTS OF THE HIL TEST BENCH :CYLINDER, DEG-HOLDER, PISTON, AND DRIVER BOX.

2.2. Motion and HV control

A MatLab® xPC Target® real-time machine is employed as the main controller of the system. Specifically, a Performance real-time target machine by SpeedGoat® is employed to run real-time routine. The device shows the following characteristics:

- Performance real-time target Intel Core 2 Duo 2.13GHz CPU, 2048MB RAM, 1024MB industrial grade SATA Flash device;
- 8 differential analog output channels, fast 16-bit analog module with (module IO108-Performance);
- 16 differential simultaneous sampling analog input channels with high-resolution 18-bit successive approximation (SAR), supporting up to 1000 KSPS per channel (module IO112-16-Performance)
- 6 x PWM generation and 8 x QAD (Quadrature Decoding) plus 1 x Interrupt and 1 x Negation (IO311-PMW6TTL/NEG1TTL/INT1TTL module).

The main functionalities of the real-time control system can be summarized as follows:

(1) run the real-time hydrodynamic model of the plant, which governs the motion of the piston, and to control the charging status of the CD-DEG;

(2) command the position of the piston that is used to induce the deformation of the ECU membrane to the motor driver (model AKD-P01206 of Kollomorgen);

(3) control the power-electronic in order to timely command the charging and discharging of the ECU;

(4) acquire the relevant data that are required to post process the experiments

(5) provide to an external scientific camera with a trigger signal to synchronize the data acquisition with the videos.

Real-time software is generated through Matlab-Simulink® and loaded on the target machine. The use of Simulink gives more flexibility and allows to perform different kinds of test easily reducing the development time of different experimental procedures. After test execution the data collected from the real time target are transferred to the PC through Ethernet communication.

Preliminary tests have been conducted in order to verify the real-time performances running a sample hydrodynamic model of a 2 Degree of Freedom (DoF) floating oscillating water column. The sample model simulation was set to:

- acquire (while running the hydrodynamic model) 8 analog differential input signals at 16-bits (only 4 of them are strictly needed for pressure and voltage measurements) and take derivatives of all of them;
- drive 4 PWM output at 100 kHz (only two are strictly required to drive the two low-voltage and high-voltage stages of the power electronics);
- drive 4 I/O ports at the sample frequency (only one is strictly required to trigger the Camera);
- 1 opened EtherCAT (bidirectional) communication channel to drive the piston motor;

A minimum refresh rate of 2 ms (corresponding to 500 Hz of sampling frequency) has been obtained, which is a value that is considered (more than) satisfactory for the representation of the dynamics of the system. However, such sample time could be further improved by customizing the EtherCAT protocol or driving the motor through analog signals.

The sensing system is composed by the following sensors:

- Voltage probes:

In order to sense the voltage on the DEG and on the primary stage of the power electronics two custom made HV probe have been implemented that features very high input resistance (nearly 50 GΩ), which drastically limits the drain of charge from the DEG electrodes, and large bandwidth, which is obtained thanks to a capacitor compensation network. In order to minimize the current leakage of the power electronics, all the HV wirings and components have been encapsulated via thick layers of silicone gel (Magic gel by Raytech) and acrylic tape (VHB 4905 by 3M®).

- Pressure sensors:

The chamber is equipped with pressure sensors that are employed (1) to collect pressure data during the operation of the device for validation purposes and (2) to implement controllers that decide the activation status of the ECU on the basis of the pressure and its derivatives.

- Camera:

In order to track the deformation of the ECU membrane, a scientific camera is employed the camera is going to be located at known position and orientation with respect to the ECU membrane. Thanks to image post-processing analysis that have been previously developed, the displacement of the tip of the membrane is going to be acquired. This is going to be used to validate models and to implement controllers that make use of the DEG displacement to decide the activation status of the ECU. A camera ECU Point Grey GS3-U3-23S6M-C with lens 250F6C, using acquisition software FlyCapture 2.9 is going to be employed.

2.2.1. Motion Controller

A conceptual schematic of the controller of the piston motion is shown in Figure 2-5.
Kollmorgen AKM52L is the servomotor that is responsible for the piston motion within the HIL . The servomotor is controlled by a servo driver AKD-P01206. The driver also manages the encoder which is integrated with the motor and the limit switches. The motion task and position profile is generated by a real-time target control unit from SpeedGoat GmbH model Performance. The control unit communicates with the driver in real time through Ethercat field bus. The same control unit reads back control parameters from the drive (position, torque, speed, status...). The interpolated position control loop is closed within the servo driver. The real-time target just sends periodically (every 2 ms) the position setpoint to the driver. The control unit is connected to a personal computer through an Ethernet cable. A Simulink model runs on the real time target with Simulink-Real-time operating system and sends all the recorded data to the PC at the end of the experiment.

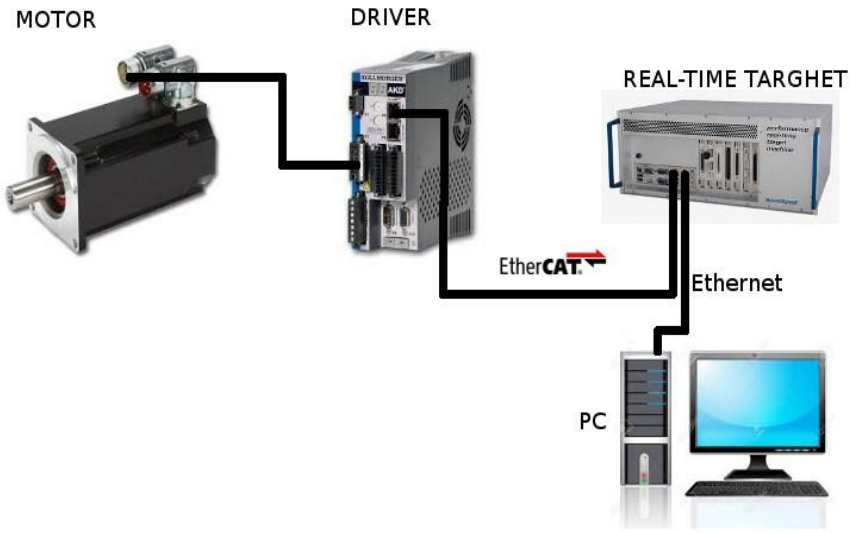

FIGURE 2-5 GENERAL SCHEME OF THE MOTION CONTROLLER ARCHITECTURE

The protocol for motor task execution is CAN over Ethercat. The Speedgoat machine is set as a master and the driver is set as a slave. The communication is established by a state flow machine, the machine starts in Init mode. Passing through pre-op and safe-op modes the state machine brings the Ethercat communication in Operational mode, as shown in the block diagram in Figure 2-6. In this state the machine is ready to operate and the Process Data Object (PDO) is synchronized and transferred bidirectionally with a fixed rate of 2 ms.
Within Simulink model the Ethercat communication is implemented by a state flow block-diagram, shown in Figure 2-7.

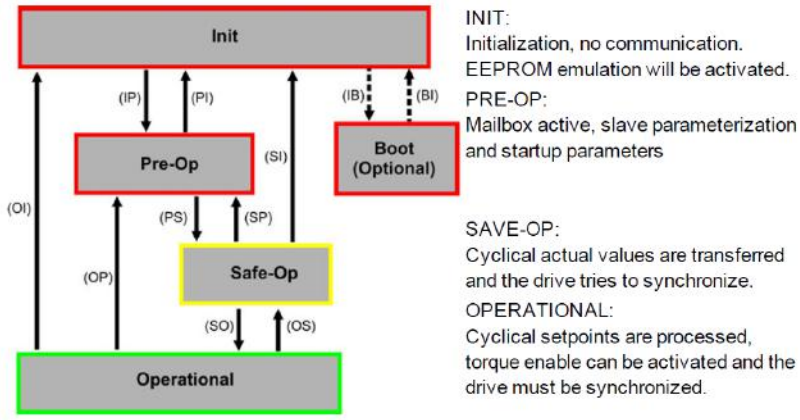

FIGURE 2-6 SCHEME OF THE INITIALIZATION FOR THE OPERATION OF THE MOTION CONTROLLER

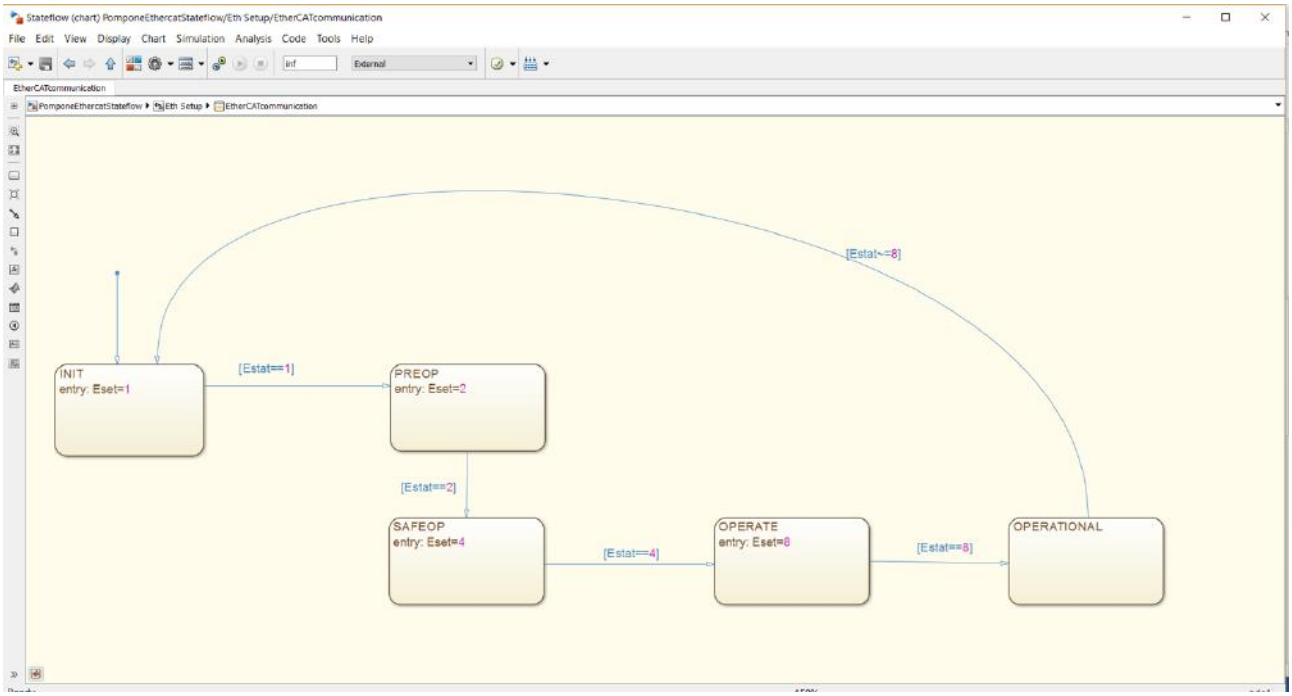

FIGURE 2-7: STATE FLOW BLOCK FOR THE ETHERCAT COMMUNICATION IMPLEMENTED IN MATALAB SIMULINK®

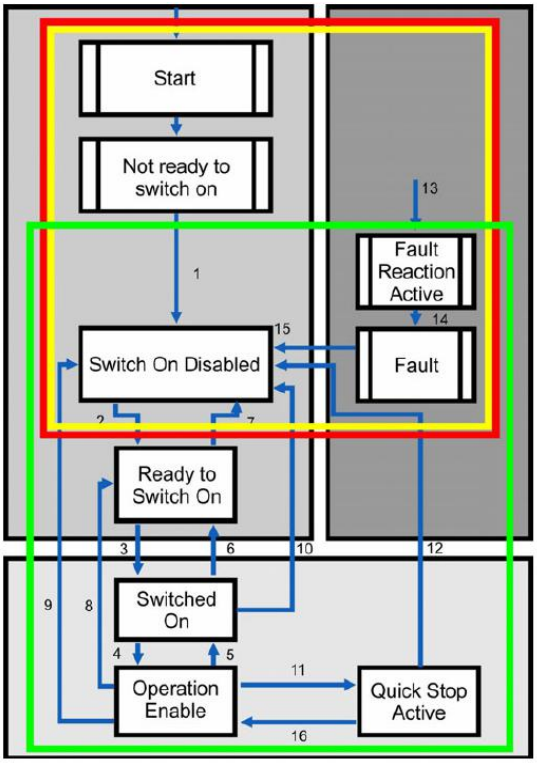

FIGURE 2-8 ETHERCAT PROTOCOL SCHEME

Ethercat protocol is used to transfer CAN messages. The state machine of CAN is shown in Figure 2-8. The behaviour of the state machine is regulated by a Satus Register and by a Control Register. Writing the Control Register we can ask the machine to skip from one block to another. Reading the status register we know in which state the machine is. The model running on the target follows a state flow machine that sends a sequence of control word values to bring the machine into 'Operation Enable' state. Here the machine is able to perform motion. The first motion task brings the piston to the home position using the negative limit switch as a reference. In this way the starting position of the piston is always halfway along the whole stroke. Once the homing position is reached the Real Time Target sends a command over EtherCAT using SDO (service data object) to bring the machine into position control mode. Here the machine performs the real HIL motion task sending periodical position setpoint over EtherCAT PDO.

In Figure 2-9 is shown the state flow of the CAN operation. In addition to normal operation, faulty conditions are also managed. Once a fault is detected the machine is no longer able to skip into operation enable state to avoid unpredictable machine movement avoiding damages to the moving parts.

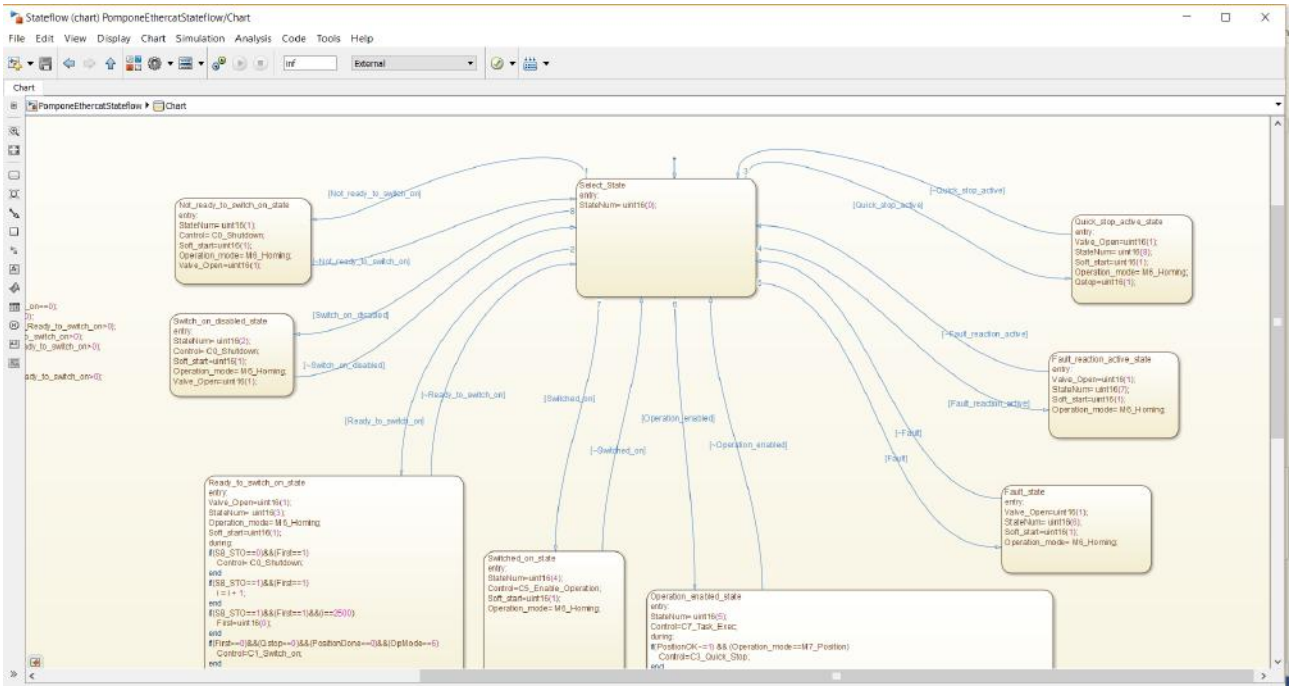

FIGURE 2-9 STATE-FLOW OF THE CAN OPERATION

2.3. HV electronics

One of the objectives of WP5 is to preliminary demonstrate the feasibility of a power electronics for the control of the DEG-PTO according to the voltage-charge *V-Q* profiles defined in Section 1 of this document.

Deliverable D5.2 reports a detailed description of a custom high voltage electronics that have been developed. In that preliminary document the design approach is described. The proposed electronics is based on the topology of the Dual Active Bridge (DAB) DC-DC converter [5][6] represented in Figure 2-10

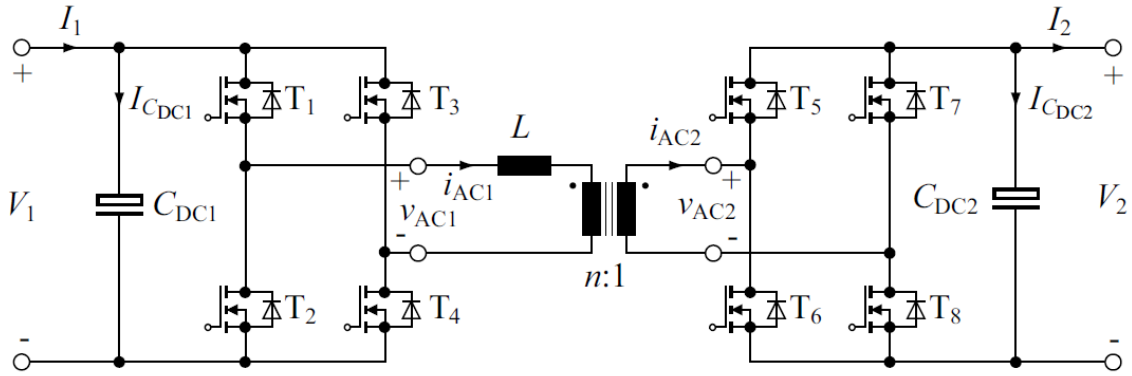

FIGURE 2-10 TOPOLOGY ADOPTED FOR THE DEVELOPMENT OF THE POWER ELECTRONICS

In the previous deliverable, a manually wired partial prototype of the electronics was described along with preliminary tests.

On the basis of such an early prototype, a full module of the HV electronics has been built and preliminarily tested. For this updated prototype, the schematic of Figure 2-10 is organized in a layout that makes use of four circuit boards, whose electronic design (represented using Gerber standard) is shown in Figure 2-11: two identical boards that includes the component of the primary and secondary respectively (power modules, see Figure 2-12); a third board the hosts the transformer and connectors and a fourth board that hosts the microcontroller. For the first Prototype a microcontroller STM32 Nucleo-64 was used to provide the control signals to the DAB.

In Figure 2-11 the custom PCB design of one of the two twin board is represented while in Figure 2-12 the different unassembled boards are shown. Finally, Figure 3.13 shows how the four boards are assembled in a compact cubic shape. This modular architecture has been chosen since it allows to introduces several changes in the design without the need of redesigning all the electronics.

For example, the transformer can be easily replaced with one with different inductance or number of turns, as well as the microcontroller can be upgraded if necessary with small effort. The modular design approach also allows to minimize the space occupation. In addition, the circuit can be scaled up easily changing the inductor up to a maximum power of approximately 0.8-1 kW.

This platform allowed us to test different solutions in terms of switching control strategies and different components in order to understand how choices influence the performance in terms of efficiency and control. Preliminary but yet promising tests conducted on this electronic system are reported in Section 4.

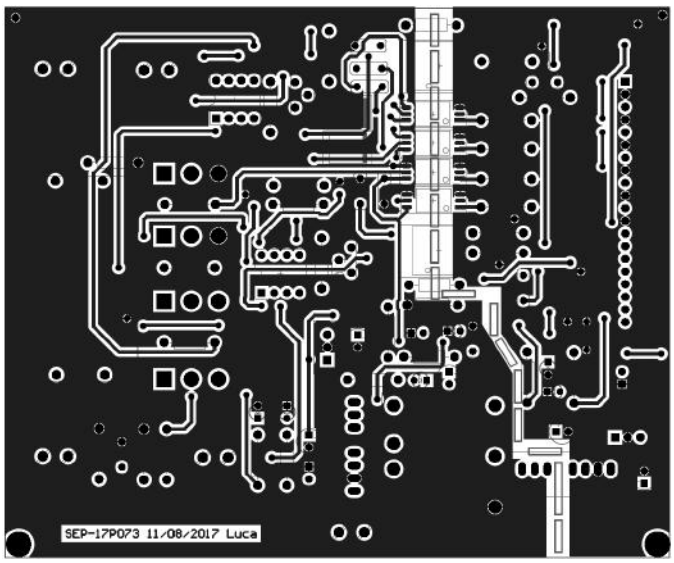

FIGURE 2-11: PICTURE OF THE GERBER FILES OF THE PCB

Microcontroller	Transformer	Inductor	Power module
	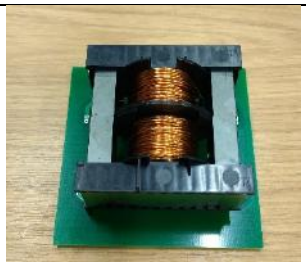		
94x96mm	94x94mm	94x94 mm	110x130 mm

FIGURE 2-12: COMPONENTS OF THE INTEGRATED MODULE-PROTOTYPE

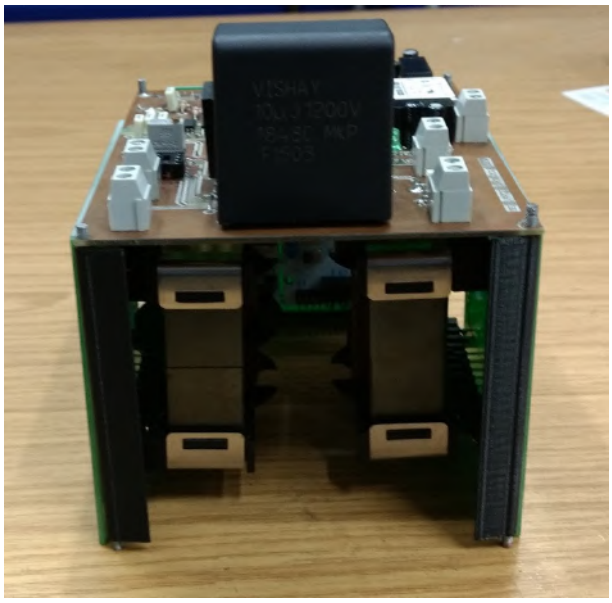

FIGURE 2-13: FIGURE OF THE FINAL ASSEMBLY OF THE HIGH VOLTAGE MODULE OF DC-DC CONVERTER

3. Manufacturing of DEG prototypes

Dielectric elastomer Generators (and also actuators) are flexible lightweight systems that can be subjected to strains of over 100%. Their core component consists of a composite elastomer made of a stack of alternating layers of electrode-elastomer and dielectric elastomer.

Effective manufacturing solutions for dielectric elastomer (DE) materials have been investigated in the field of actuation technologies (i.e. DE working principle employed as actuator, to convert electrical energy into mechanical energy). Few works are oriented to the manufacturing of generators. Most of the previous works are basically oriented to the manufacturing of small scale devices (millimetre or centimetres size) according to different techniques. In the context of this project, we aim at defining a manufacturing technique that can be potentially scaled up to larger power size.

In this section, we analyse different possible manufacturing techniques and implement them in order to develop a novel prototype of DEG-PTO. Additionally, we discuss the selections among the possible procedures suitable for the purpose of this project and for future developments.

Finally, we have implemented a set of experiments and procedures to build different prototypes of DEG-PTO that are integrated with the testing setup described in Sect 2 and tested in a series of experiments described in Sect.4.

3.1. Manufacturing techniques

This subsection provides an overview and analysis of existing manufacturing techniques for the two main elements that compose the ECU within a DEG-PTO i.e. dielectric elastomer layers and electrodes.

3.1.1. Manufacturing of dielectric layers

Dielectric layers of a Dielectric Elastomer Generator are the core component of this PTO system. The electrostatic generation principle illustrated in the previous section of this deliverable is in fact based on the capacitance variation of a capacitor in which the DE acts as the insulating layer.

The electrical and mechanical properties of the DE membranes can strongly affect the performance of the DEG. Specifically, DE layers employed for the fabrication of DEGs must have the following characteristics in order to guarantee an effective operation [7].

- Dielectric strength:

  The energy that can be converted in a cycle of operation of a DEG that is approximately proportional to the square of the working electric field. Thus, a DE membrane with higher dielectric breakdown field can guarantee the conversion of more energy per cycle or makes it possible to obtain the same converted energy with the employment of less material (i.e. reduced cost of investment). Dielectric strength of materials that are typically employed as DEs range between 70 and 100 MV/m.

- Dielectric constant:

  In general, high values of the dielectric constant are desirable for DEGs as for a given value of the breakdown field the effective amount of converted energy is directly proportional to the dielectric constant of the material. Typical values of the relative dielectric constant for common DE materials are in the range of 2-5. Possible increase of dielectric constant can be obtained by introducing different type of fillers but the introduction of this particles usually has a detrimental effect on the

dielectric strength. A high dielectric constant would be also desirable to increase the electrical time constant of the material (see "conductivity and time constant" item below).

- Strain

The condition of mechanical rupture of the polymeric material can be expressed as a limitation on the maximum allowed value of the stretch within the material. DE materials exhibit large values of limiting stretches (in the range of 400-800 %). A large value of maximum stretch is desired since the amount of convertible energy increases with an exponent that is usually between the square and the cube of the maximum stretch. Typical values of rupture stretch for common DE materials are: 500-600 % for natural rubbers, 400-500 % for styrenic rubbers; 300-400 % for silicones and 700-800 % for acrylics.

- Conductivity and time constant:

During the operation of DEGs, the DE layer is subjected to high electric field of up to a relevant fraction of its dielectric strength. At these high levels of electrical loading the DE membrane must be able to limit the leakages of charge since this contributes to generate inefficiencies (see simulations conducted in Deliverable D5.1 for more details). Thus, the DE material must possess a high resistivity (ρ). More specifically, the relevant property is the electrical time constant of the material that reads as $\tau = \varepsilon\rho$, where ε is the dielectric constant. As shown in simulations reported in D5.1 a time constant of 10 s or more must be guaranteed to limit inefficiencies. Time constant of typical materials employed as DE are in the range of 10-100 s except for the VHB which tend to have values below 5-8 s.

Relevant material properties are reported in Table 1. It is worth noticing that a membrane layer is likely to achieve such properties if it is manufactured appropriately. The fabrication process has an influence on most of the above-mentioned parameters but most relevantly it has crucial influence on electrical breakdown and ultimate stretch.

TABLE 1: RELEVANT MATERIAL PROPERTIES FOR DE LAYERS OF DEGS

Material	Dielectric strength (MV/m)	Relative Dielectric constant (-)	Maximum Stretch (%)	Resistivity (Ω/ m)	Time constant (s)
Natural Rubber	80-100	3	500-600	10^{12} - 10^{13}	20-100
Styrene Rubber	80-100	3	400-500	10^{12} - 10^{13}	20-100
Silicone	70-90	2.7	300-400	10^{12} - 10^{13}	15-80
Acrylic (VHB)	70-100	4.2	700-800	10^{11}	3-10

3.1.2. Manufacturing of deformable electrodes

The electrodes of DEGs have a relevant impact on the device's performance: they must be conductive, yet they must be soft (in order not to add stiffness contributions); they must sustain large deformations while remaining conductive, yet they must be able to do so for millions of cycles. The life of a compliant electrode for DEGs is currently a bottleneck, and it comes as no surprise that the "perfect" electrode has yet to be developed. However, much progress has been made from the first reported devices whose electrodes were hand-painted carbon grease, and over the years, creative new methods and technologies have started to emerge.

The electrodes of a DEG are subject to the same amount of deformation as the polymer and must consequently sustain strains typically of up to 100 % without being damaged and while remaining conductive. Their mechanical impact on the stiffness of the dielectric must be low to avoid introducing unwanted stiffness. The ideal electrode would be highly conductive, perfectly compliant and patternable, and could be made thin relative to the polymer thickness.

A first trade-off found in early works is to use electrodes based on carbon powders applied with a brush or a spray. Graphite and carbon black powders, conductive carbon grease, or carbon powders in an elastomeric matrix are the most technically advanced and diffused types of electrode, because of their low stiffness and ability to remain conductive at large strains.

The carbon-based electrodes can be categorized in three main variants:

a- loose particles of carbon;
b- carbon grease, which consists of carbon particles dispersed into a viscous media such as oil;
c- conductive rubber, which is formed by dispersing carbon particles into an elastomer, which is crosslinked after it has been applied on the membrane.

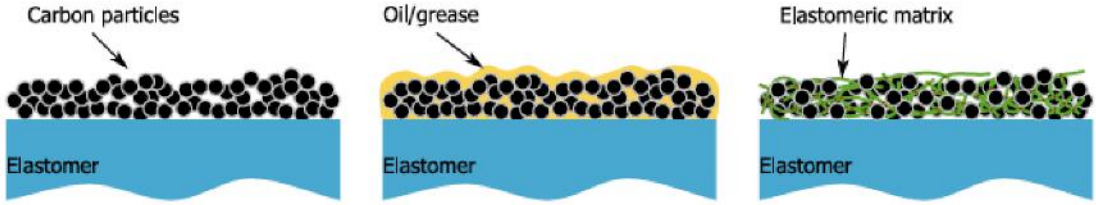

FIGURE 3-1: SCHEMATIC REPRESENTATION OF THE THREE TYPES OF CARBON-BASED ELECTRODES

Carbon particles

One of the main advantages of powder-based electrodes is that they do not contribute to the stiffness of the membrane on which they are applied, due to the absence of a strong binding force between the agglomerates. Loose carbon powders (mainly carbon black and graphite), directly applied on the dielectric membrane, were thus the material of choice in the early prototypes, as they allow demonstrating the large strain capabilities. It worth noticing that carbon is usually preferred over metal powders, although metals are intrinsically more conductive than carbon, but their powders have a tendency to form an insulating oxide layer at the surface. Additionally, metal particles are too large to create sufficient contacts, and a better conductivity can be obtained with carbon particles. Metallic powders are therefore rarely used for DE transducers, although a few attempts have been reported using silver grease electrodes . The relatively high electrical resistance of carbon-based electrodes does not play a primary role for DE actuators, as long as the electrical time constant of the device remains smaller than the mechanical bandwidth. For instance, a 1 cm^2, 40 µm thick DEA with a silicone membrane has a capacitance of about 65 pF. With electrodes whose resistance would be in the MΩ range, it could still be driven up to 1 kHz. In addition to being quite difficult to handle due to their high sensitivity to static charges, loose powders present several disadvantages: maintaining full coverage at large strains is difficult, and the lifetime of the electrode is limited due to the possibility of the conductive particles to detach from the electrode. Consequently, electrodes with loose powders are mainly found in combination with adhesive acrylic elastomers (such as VHB from 3M) as dielectric layer: because this material is intrinsically sticky, the conductive particles become bounded to its surface. A notable exception where loose graphite powder electrodes are used in combination with a silicone elastomer is in the multilayer process. In this case electrode is effectively covered by the next dielectric layer.

Carbon grease

One way to solve the issues mentioned above is to bind the powders into a viscous matrix, such as grease. Although easier to handle than loose powders and capable of sustaining larger strains while remaining conductive, carbon-grease electrodes also have disadvantages: grease can have long term stability issues caused by drying or diffusion into the dielectric membrane, which can cause short circuits or swelling of the elastomer membrane. As any viscous material, grease also creeps under gravity, which negatively impacts the lifetime of these electrodes, particularly for devices stored vertically. The absence of a reliability study on these kinds of electrode (and DEAs in general) makes it difficult to assess the importance of these factors. Furthermore, grease, similarly to loose powder, can be subject to mechanical abrasion, which also negatively impacts the lifetime. Carbon grease electrodes was the first solution employed for early prototypes of DEG-based WEC developed in the framework of the project PolyWEC.

Conductive rubber

Finally, the conductive carbon black particles can be incorporated into an elastomer matrix, such as a silicone, which is cured after the electrode is applied on the membrane, in order to obtain a polymer-carbon conductive composite. Because in that case the electrode is bound to the membrane, it is much less prone to ablation or migration of the electrode material with time, which positively impacts the electrode's life expectancy. However, because of the elastomeric matrix, the electrode's contribution to the stiffness of the elastomer cannot be neglected anymore, compared to carbon powder or grease. As Pelrine et al. pointed out, these types of electrode work best for thicker dielectric films, i.e. when the thickness of the electrode is negligible in comparison with the thickness of the dielectric elastomer [8]. The stiffness of an elastomer carbon black compound is very dependent on the quantity of filler particles, which must be sufficiently high to be above the percolation threshold. The percolation threshold is very dependent on the surface area of the carbon black, as well as the matrix in which it is dispersed and can vary between 1 and 24 % [9]. In silicone, we have observed a percolation threshold of about 6 % for Ketjenblack EC-300J from AkzoNobel, and of about 3 % for Ketjenblack EC-600JD, due to its extremely high surface area (1400 m^2/g according to the datasheet, compared to 800 m^2/g for the former). With graphite (4206 from Merck) in DowCorning Sylgard 184, Kofod observed a percolation threshold of 23 % [10]. Assuming the same silicone is used to produce the dielectric membrane and the conductive electrodes, the mechanical stiffness of the filled polymer will be larger than the membrane's, thus showing the importance to apply the material in a very thin layer. The main carbon-based compounds reported in literature for the fabrication of compliant electrodes for DEAs are summarized in Tables 1, 2 and 3. In addition to these three main types of carbon electrode for DEAs, some other ideas have been presented, for example using carbon nanotubes (cf. Sect. 5.3) or exfoliated graphite [11].

Application methods for carbon electrodes

While simple prototypes and demonstrators can be manufactured without much regard of the shape, precision and thickness homogeneity of the electrodes, which can simply be smeared on the elastomeric membrane, a device for commercial applications require electrodes of a precise shape, patterned on a cm or mm scale. Several techniques can be used to apply and pattern carbon electrodes on a dielectric elastomer:

- A shadow mask, or stencil can be placed on the elastomer membrane to selectively expose the surface that needs to be coated with the conductive material. If the thickness homogeneity and reproducibility is not a main concern, the conductive solution can be simply applied on the mask

with a brush. For better uniformity, spray coating can be used in combination with a shadow mask to apply a thin uniform layer on the elastomeric membrane. For their automatized stack process, it has been tested spray coating through a shadow mask of both dry graphite powder and graphite in suspension in isopropanol [12]. With this process, which alternates between the application of a silicone layer by spin coating, the heat-activated cross-linking of the silicone, and the subsequent deposition of the electrodes, an efficient production method can be obtained, which allows building actuators of up to 100 layers with a production time of 5 minutes per layer, thus demonstrating that carbon electrodes can also be used for larger scale and commercial applications. A similar stacked actuator fabrication process with a sequence of silicone and electrode deposition by spray coating with an airbrush [13]. Because the dielectric layer is also sprayed, there is no need for a spin-coater, thus reducing the cost of the installation. Their electrode consists of graphite powder put in suspension in a solvent (1:4 ratio).
As it will be seen in the following the production methods that was chosen for the development of the ECU of the DEG in this project is based on shadow masking technology.

- Spray coating through a shadow mask can also be used with conductive rubber if mixed with solvent to decrease viscosity [14]. One drawback of using a stencil to define the shape of the electrodes is the contact between the mask and the elastomer membrane, particularly in the case of very thin suspended membranes. If applying the mask and spraying the electrode can be done quickly, removing the mask at the end of the process must be done slowly and carefully in order not to damage the membrane stuck on the mask. Leaving a small gap between the mask and the membrane is not advisable because shadowing will occur at the mask border and the airflow from the spray coating system can deform the membrane, leading to a loss of resolution. Stamping patterned structures can also be obtained by stamping the conductive electrode on the dielectric membrane. A soft stamp with the desired pattern is fabricated, for example by replication on an etched silicon negative master. Small structures and a good resolution can be obtained with this method. Stamping loose carbon black powder is made possible for particular application that employ VHB adhesive as dielectric layer: the stickiness of the surface ensures the transfer of the carbon particles from the stamp to the membrane, and fixes them on the elastomer surface. Commercially available stamping techniques can also be used with carbon grease or conductive rubber when adequately diluted to form a conductive ink.
- Printing techniques. A further technology for the manufacturing of electrodes is the inkjet printing. Different types of carbon electrode can be prepared in the form of a conductive ink, and most of the techniques developed for the printing industry, including inkjet printing, screen printing or roll-to-roll processes, can be applied to pattern conductive electrodes on elastomers. The polymer solar cell community, for example, is using these printing methods for the manufacturing of flexible devices. Their production lines require high throughput, the coating of large surfaces, and the patterning of precise features (down to the µm scale). This is similar to the needs of compliant electrodes for DEAs in case of a large-scale commercial application. Among the standard printing methods, inkjet printing is particularly interesting, because it is a purely non-contact method, and it is therefore well-adapted for thin suspended membranes. This is a versatile method, as the shape of the electrode can be adapted at will just by modifying the bitmap used to print the electrode. This represents a very interesting advantage over shadow masks for the research community, because different designs can quickly be printed and tested. Large-scale printers with multi-nozzle (up to 1000) printheads are capable of large throughput, which renders this technique also attractive for commercial high-volume production. A major difficulty resides in the development of a jettable ink for EAP applications, which is not a straightforward task. The parameter space is limited by a large number of factors: first, there are the printer/nozzle requirements on liquid viscosity, surface tension and vapor

pressure, which must be followed in order to obtain regular and stable generation of drops on demand. These requirements are nozzle-related and can be quite tight. For example, the R&D printer Dimatix DMP-2800 from Fujifilm requires inks with viscosities between 10 and 12 mPa·s, and surface tension between 22 and 33 mN/m. To avoid clogging the small nozzle orifices (typically 10–100 μm depending on manufacturer), the carbon particles must be carefully dispersed and no flocculation or sedimentation is allowed. The evaporation rate of the ink must not be too high, to avoid clogging the nozzle when it is not jetting (i.e. when the nozzle is traveling above a zone which must remain free from ink). Secondly, the interaction between the droplet and the membrane, once the former reaches the latter, adds further requirements on the fluid formulation. The contact angle between the ink and the elastomer must be low enough to obtain good wetting. If the contact angle is too high, there is a risk that adjacent droplets merge together and form a large ink pool, causing a dramatic loss of resolution. This is especially problematic with silicones, which have a very low surface energy and present highly hydrophobic surfaces. Different surface treatments (plasma activation, UV exposure) can help to temporarily increase the surface energy, and Robinson et al. have recently demonstrated how the wetting of a silicone substrate by a solvent-based ink can be improved by structuring the silicone substrate with micropillars [15]. The ink's evaporation rate must be controlled so as to avoid the "coffee stain" effect, which is caused by the motion of the ink's solid content to the periphery of the droplet, leading to a non-uniform coating once the layer is dry. This effect can be avoided by carefully choosing the solvents used for the ink formulation, using a mix of solvents with different vapor pressures [16]. Finally, the ink formulation must be selected so that the dry and cured film fulfils the requirement for compliant electrodes: low stiffness, compliance, conductivity etc.

3.1.3. Choice of materials and manufacturing technique

One of the objective of the WP5 of WETFEET is to develop a first prototype of intermediate scale (20-40 cm) of an integrated DEG which shows several of the characteristics of a scaled pre-commercial prototype even if it is produced at laboratory scale. To this aim, a consistent fabrication procedure has been designed in order to: (1) produce this first intermediate scale prototypes (20-40 cm); (2) demonstrate a fabrication process that can be potentially and effectively scaled up for the production of large scale systems (of meters scale in dimensions).

The choice of the dielectric materials has been oriented to novel developed DE films commercialized by Wacker Polymers and Parker Hannifin. These are two silicone-based films produced purposely for the development of actuators, generators and sensor made of DE that have been recently put on the market by the two multinational companies. They are available in batches of different thicknesses and widths. The choice of a commercial film, even if suboptimal for certain available material properties, is considered the current most promising way of obtaining a reliable system which shows performance that are close to a pre-commercial PTO prototype (even if at smaller scale). These commercial materials are in fact produced according to high quality industrial standards that can guarantee reliability, repeatability and high performance of the system. Additionally, they are already produced at industrial level with high production volume capabilities demonstrating the manufacturability of these systems.

As it was reported in deliverable D5.2, Wacker Elastosil films have been successfully employed for the development of different smaller scale ECUs for DEG-PTO, obtained by applying deformable electrodes on commercial film of 100 μm in thickness. These preliminary prototypes have been tested on a small scale setup showing very promising results in terms of energy density and efficiency.

For larger scale prototypes, we envisaged the employment of the DE film commercialized by Parker which is available in rolls of 1.4 m in width. Unfortunately, the process and the materials that were designed to apply electrodes to the Wacker film was not exportable to the Parker film. This is due to the bonding of the electrode on the silicone film which was not strong enough to guarantee an appropriate operation. Thus, in order to manufacture the prototype to be tested within the larger scale HIL setup, we have (successfully) produced custom silicone films starting from different commercial liquid silicones, that have been blade casted and crosslinked (i.e. processed to become a rubber-like material) according to the procedure described in the following sections. On the one side, this can be considered as a limit of our investigation, but on the other side this gave the opportunity to demonstrate that effective films made of silicone can be obtained with a relatively simple fabrication process that can be implemented without using specialized equipment. This shows that the success of the future scaling up of the system is less bounded to the available commercial product since their fabrication processes are quite replicable.

As for electrodes, among the analysed techniques for their manufacturing, the shadow masking technique has been selected as the most effective and reliable technique for the manufacturing of a relatively large ECU prototype. Specifically, the choice was oriented to a shadow masking fabrication procedure in which the liquid electrode is poured directly using a shaped mask and then crosslinked in air or in oven (the process will be described in detail in the following). This technique allows to achieve the accuracy and the quality of a commercial product but keep the complexity of the equipment low enough.

Other electrode fabrication techniques were excluded for the following reasons:

- Spray coating:

  Spray-coating can be an effective technique for the application of electrodes, however it has been considered not suitable for large scale system manufacturing. The main reason is connected with the relatively low manufacturing throughput that could be reached at larger scale.

- Printing:
  Printing could be effective but requires a specialized machine to be developed for large scale production which would feature multi head printing systems to increase the production throughput. This would require the development of a custom printing-machine that can be in the long term but not for a first pre-commercial prototype.

A further step toward the commercialization would be the definition of a faster and more repeatable process that can be adapted for large volumes productions.

3.2. Preliminary VHB prototype

A first prototype of ECU has been developed in order to replicate a prototype that was originally developed in a previous research project. This is made for the purpose of validation of experiment as explained in detail in Section 4.

The reference ECU is as the inflatable circular diaphragm as described in Section 1 that undergoes out of plane expansion when its opposing sides are subjected to a pressure difference. The design and optimization of the complete and fully functional setup for the small-scale DEG-PTO has been initiated from the preliminary dimensioning of the system. The aim is to obtain appropriate system dimensioning with a rational scaling of its dynamic response.

Our design strategy started from the definition of a nominal power generation requirement of the DEG. A target nominal power of W_N=5 W was chosen that is a representative of a scale between 1:15 and 1:20 of a 100-200 kW real device. The maximum working voltage has been chosen of real scale devices is foreseen to be in the range of 10-30 kV. For this scaled prototype 10 kV has been chosen as a trade-off. Such a value is enough to effectively represent/demonstrate the real scale issues of electronics and components, but at the same time it does not set very strict requirements for the safety of the laboratory setup. Once the target power and the working voltage are decided, it is possible to define the target capacitance of the ECU. In particular, considering that the capacitance is changing roughly by four times from the initial value (flat membrane) when the membrane is fully inflated, a choice of a minimum capacitance C_{dm}= 50-100 nF and a maximum C_{dM}= 250-500 nF lead to the required energy converted per cycle.

The same capacitance variation can be obtained with different combinations of thickness and radius of dielectric layers. From the electrical point of view the choice is rather free, on the contrary from the point of view of the dynamic response this choice can have great effect on the corresponding real scale device. The problem has been previously studied and the result bring to optimal combination of thickness/radius that are quite different with (1) the type of WEC device; (2) with employed DE materials, (3) with initial pre-stretch of the membrane. In any case the following dimensions of the membrane allow to implement a sufficiently accurate (small-scale) representation of most of the combination of materials and devices:

Diameter: 0.35-0.45 m

Thickness: 0.1-1.0 mm (one up to four layers of dielectrics)

Manufacturing

A first prototype of DEG-PTO has been manufactured using VHB acrylic. A 1 mm thick acrylic elastomer film has been employed as single dielectric layer. The DE is manually pre-stretched of a factor 3 and attached on a circular frame with internal diameter of 0.39 m. Conductive deformable electrodes are obtained by manually depositing a mixture of silicone and carbon black powder (Figure 3-2a). The obtained DEG-PTO has an initial capacitance of 50 μF. The DEG membrane is mounted on the DEG holder (see Figure 3-2) and inflation/deflation tests have been performed. During the deformation, a maximum capacitance variation of a factor 5.3 has been recorded.

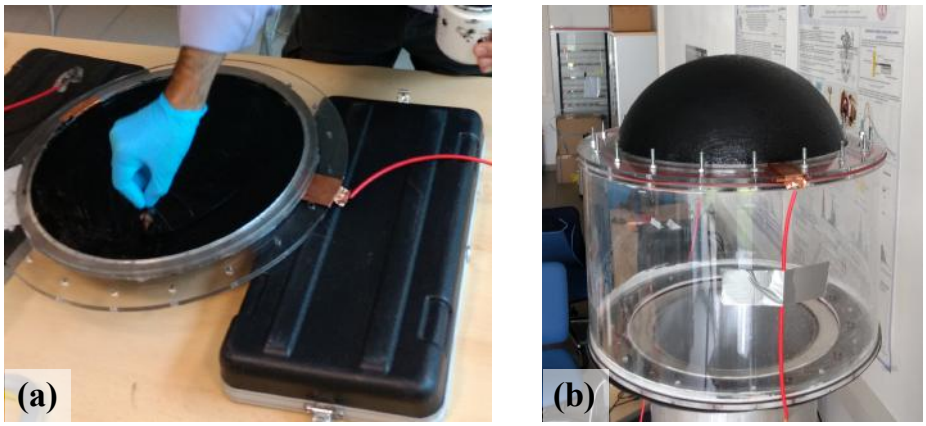

FIGURE 3-2 DEG MEMBRANE PROTOTYPE: PREPARATION PHASE (A) AND DURING THE TESTING (B)

3.3. PDMS DEG-PTO manufacturing

This subsection describes the manufacturing of an advanced DEG concept, based on optimised silicone materials and on a scalable multi-layer layout. Compared to previous DEG prototypes, the presented materials and topology represent a scalable solution which allows potential scaling-up of the DEG technology.

Since DEGs are manufactured using compliant elastomers, they can be shaped into many configurations over a wide range of dimensions.

The most common configuration is using a single layer generator, but in order to meet the requirement of frequent inspection and possible DEG replacement, it is advisable that the first full-scale DEG PTOs feature modular architecture, as reported in Figure 3-3.

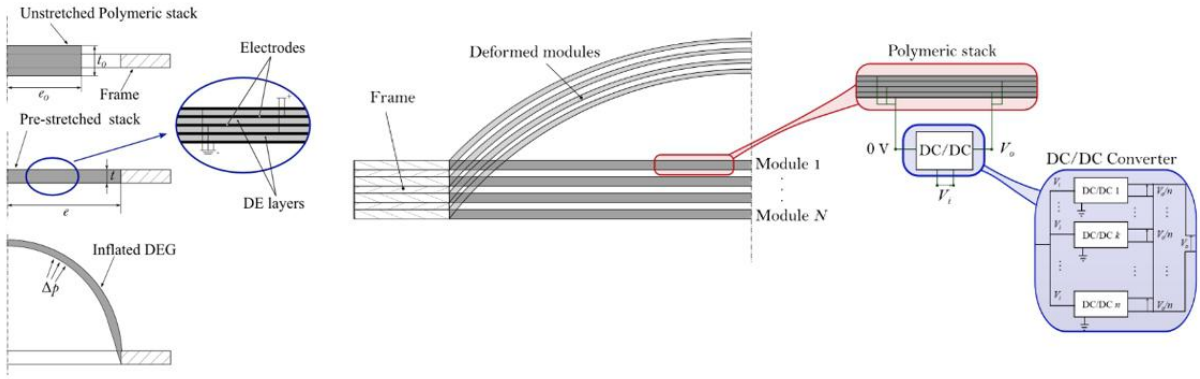

FIGURE 3-3 SCHEME OF THE DEG PTO ARCHITECTURE WHICH HIGHLIGHTS THE MODULAR STRUCTURE.

In this concept, each PTO is partitioned into *N* independent modules which are physically separated (e.g., spaced by a fluid) and can be accessed/replaced individually in case of failure. Each individual module has a multi-layered architecture in which the single DE layers are coated with compliant electrodes and electrically connected in-parallel. Each module is equipped with a DC-DC converter, capable of providing bidirectional electricity fluxes, and featuring the architecture shown in Figure 3-3**.**

The multi-layered architecture allows the implementation of large electric fields within the DE layers (thus enabling large convertible energy density), while limiting the applied voltage. In the following, material selection, procedures for manufacturing, pre-stretching and layers stacking are discussed.

3.1.1 Materials

A great effort has been invested in the development and optimisation of elastomer materials used for the dielectric layers [17]. Synthetic and natural rubbers, acrylics and polydimethylsiloxanes (PDMSs), commonly referred to as silicones, are some of the most used. In particular, acrylics and silicones are very promising for their excellent capability of undergoing large strains without damaging.

Previously, a commercially available acrylic elastomer (VHB 4910 from 3M) with high strain performance (up to 400 %) and high theoretically energy density (about 3.4 MJ/m^3) has been used. Unfortunately, these acrylic films have large viscoelasticity and insufficient resistivity which negatively affects the energy conversion performance of the dielectric elastomer generator. Furthermore, the requirement of having highly flexible and long-lasting electrodes influenced the elastomer choice.

Acrylics are intrinsically sticky, thus carbon powders or greases electrodes are directly deposited on the dielectric film. Both have good conductivity, even at really high strains especially in the case of carbon greases, and since they create weak binding forces between the agglomerates, they do not affect the stiffness of the dielectric membrane, but do negatively affect the lifetime of the final generator.

A comparative evaluation of some of these kind of electrode materials was performed in [11]. The authors demonstrated as, although well adapted to lab experimentations, these electrodes exhibit poor structural stability which limits the integration of such generators into real systems. Silicones, besides of having lower viscoelastic effects, allow to make compliant electrodes which are very interesting for their high life expectancy. In addition, the use of the same matrix for the different layers of the DEG will improve the interface between the insulator and the conductive layers. In [18] Vu-Cong et al. showed that when the nature of the polymer constituting the electrodes is the same as the nature of the electroactive polymer used for the application, the change of the dielectric constant is minimal. Thus, silicone elastomers have been chosen to be used both for the dielectric layer and the compliant electrodes matrix.

Compliant electrodes, made by dispersing conductive particles (such as carbon black or graphene) into an elastomer, are very promising [19]. Conductive particles can be integrated into an elastomer matrix obtaining a polymer conductive composite, which is less prone to ablation or migration of the electrode material with time because of its mechanical and electrical bound to the dielectric. With this technique, the electrode's contribution to the stiffness of the elastomer cannot be neglected anymore, compared to carbon powder or grease. The stiffness of the silicone-conductive particles compound is strongly dependent on the concentration of the filler that need to be as low as possible not to increase it, but at the same time it has to be above the percolation threshold to obtain a conductive composite material. Thus is preferable to use filler particles with low percolation threshold. The threshold level is very dependent on the surface area of the conductive particles, besides the matrix in which it is dispersed, and it can vary between 1-24 %.

The conductive fillers investigated in recent years are mainly carbon-based nanocomposites because of their outstanding dielectric permittivity [20] and superb electrical conductivity [21]. Typical examples of carbon nanofillers include carbon black (CB) particles [10], carbon nanotubes (CNTs) [22], carbon nanofibers (CNFs) [23], and graphene nanoplatelets (GNPs) [24]. CBs are an amorphous form of carbon with a structure similar to disordered graphite and are the most used in literature as conductive filler mainly because they are cost effective. When used as conductive filler, CB is characterized by three major properties: particle size (surface area), structure, and surface chemistry. Among different CBs we chose the Vulcan XC-72 from Cabot, because it is characterized by a high surface area that, decreasing the gaps between the polymer and the conductive aggregates, allows to reach a high conductivity even at low particle loading.

Silicones are available in a large range of stiffness and compositions, which gives design freedom and the possibility to easily mold them in various geometries. Furthermore, they are usually sold in a viscous base form that can be applied in thin-membranes. This provides yet an additional degree of freedom because the thickness of the membrane can be freely chosen and it is not imposed by the manufacturer as in the case of premade films, mainly acrylate films as the VHB products [2][25][26].

3.4. DEG-PTO manufacturing procedure

This sub-section illustrates the fabrication process of DEGs that has been conceived and studied in order to produce a functional and reliable DEG-PTO to be employed in the test campaigns.

Generally, concerning the dielectric membrane of a DEG, it is more advisable to use silicone films fabricated with high accuracy and controlled environment conditions, in order to assure the quality and the uniformity of the dielectric layer. Indeed, as a matter of fact, DEG's lifetime is strictly related to the quality of the dielectric elastomer. Lifetime is shorter in the presence of defects inside the elastomeric material, like external bodies, inclusions or micro voids. Therefore, it has been chosen to adopt and purchase dielectric materials already fabricated.

Recently, some multinational companies, such as Wacker GmbH or PARKER, have released commercial DE films with the high-tolerance requirements mentioned above. Both those companies manufacture dielectric films that have been considered for the DEG manufacturing procedure described in this document for the following reasons:

(1) Wacker and PARKER films are the first commercial products that have been purposely developed for the application of DEGs;
(2) They are silicone-based products that make it possible the integration of silicone-based conductive electrodes;
(3) The material's performances (from datasheet) are very promising in terms of dielectric constant and electrical break-down limit.

We should however underline that the current costs of these materials are probably too high to be eligible for an effective economic deployment of DEG-based WEC. Nevertheless, we have also to consider that the current production costs are those of a prototype material for niche laboratory applications, and a drastic cost reduction could be determined by future economy of scales. The dielectric elastomeric membranes of those two companies which are suitable for DEG applications are:

- Wacker: Elastosil silicone film, available directly in rolls with width up to 250 mm.
- Parker: elastomeric film with width up to 1.4 m.

Pictures of those products are reported in Figure 3-4.

FIGURE 3-4: WACKER AND PARKER DIELECTRIC FILM

For the purpose of this project, the fabrication process of a DEG transducer has been designed for both small-scale laboratory tests and large-scale experimental tests.

The most suitable elastomeric film for the application is the one from Parker, because of its excellent dielectric characteristics and especially for its large commercial width (1.4 m).

Despite those features, electrodes manufacturing tests revealed that, with the established manufacturing procedure described in this document, no adhesion on the dielectric membrane was achieved, probably due to the employed electrode composition which does not fit well with the Parker film.

Thus, in this project, the Wacker Elastosil film with un-stretched thickness of 200 μm has been used for small scale test. Indeed, on such films, successful deposition of silicone electrodes (made of Elastosil RT 625 A/B, a Wacker product in viscous base form) has been achieved.

Whereas, considering the large scale experimental tests, since commercial Elastosil films have a too small width (250 mm), custom dielectric films have been prepared in laboratory using the same Wacker blend employed for the electrodes (Elastosil RT 625 A/B), allowing to prepare custom-made dielectric membranes whose thickness and width can be freely chosen.

3.4.1. Electrodes manufacturing procedure

The electrodes are prepared and deposited on the DE layers using a procedure that is described in the following [27]. During the deposition procedure, the dielectric film is firmly fixed on a flat surface. The electrodes are deposited successively on the two sides of the dielectric. The different phases of electrodes deposition are schematically represented in Figure 3-5.

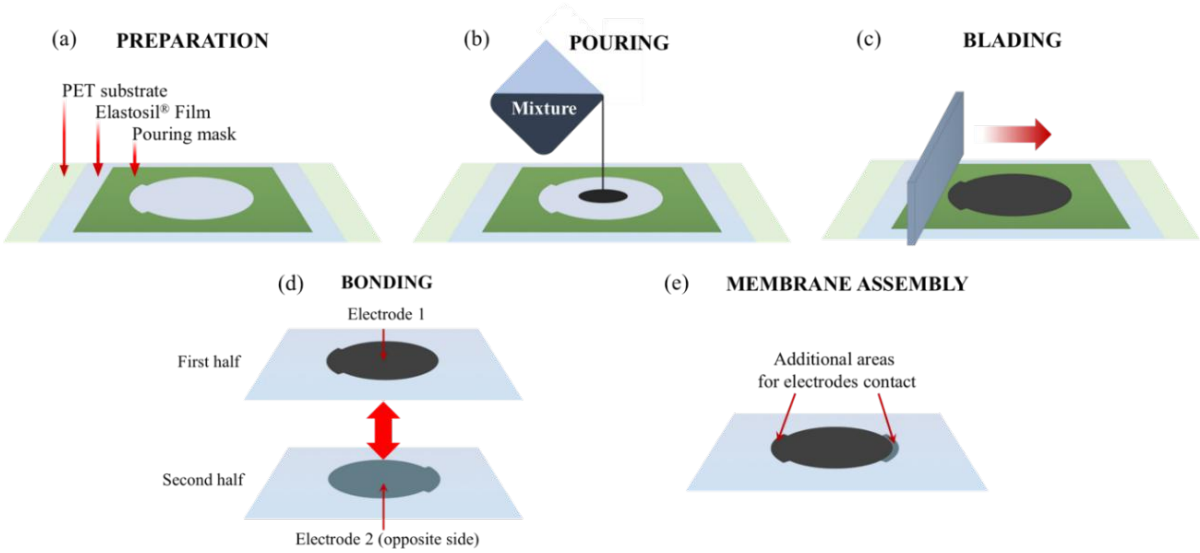

FIGURE 3-5: PHASES OF THE PREPARATION OF THE ELASTOMERIC ELECTRODE ON A COMMERCIAL ELASTOSIL DE FILM: (A) POURING MASK WITH SHAPED CUT IS LAID ON THE ELASTOSIL® FILM (THAT IS KEPT ON ITS PET SUPPORT), (B) MIXTURE OF PDMS, CARBON BLACK AND ISOPROPANOL IS POURED; (C) THE EXCESS OF MATERIAL IS REMOVE

The conductive layers are prepared starting from a dense liquid compound that is poured directly on top of the dielectric film using a plastic mask to obtain the desired electrode shape and thickness. The mask and blade used in the tests campaigns are presented in Figure 3-6.

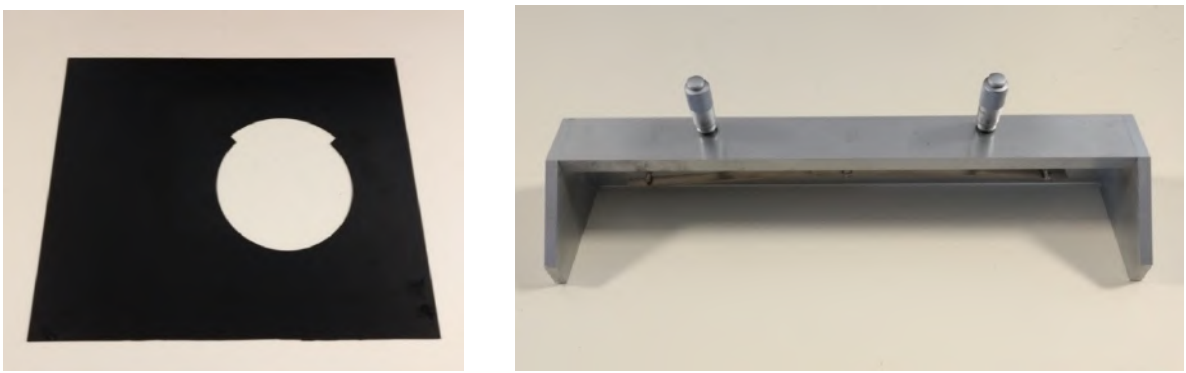

FIGURE 3-6: PICTURES OF THE TOOLS THAT HAS BEEN EMPLOYED FOR THE PREPARATION

The electrode compound is liquid when poured, for this reason the substrate must be fixed on a flat surface which is kept horizontal until the compound is completely polymerized in order to obtain a uniform thickness conductive layer. The polymerization of the compound is accomplished in about 12 hours at ambient temperature. Within this time the electrode loses more than ¾ of the original thickness. To obtain an electrode 80 – 100 µm thick the required original thickness of the mask is 400 µm. At the end of the polymerization the conductive layer is perfectly bonded to the dielectric substrate. After pouring the compound on the mask, a blade is used to spread the compound and remove the excess of material in order to obtain a uniform thickness of the electrodes. This process is successively repeated on the two sides of the dielectric membrane.

As previously mentioned the electrode compound is made dispersing CB particles into a silicone matrix. To do that, a planetary shaker machine has been employed. During the operation, isopropanol (IPA) solvent has been used, to increase the fluidity of the carbon powder-silicone mixture during the mixing phase.

The fabrication process can be summarized in the following steps (quantities are relative to the fabrication of a single electrode sample with 105 mm diameter and thickness of 80 μm):

1. Put the planetary shaker container on a scale.
2. Mix carbon black powder with IPA solvent and certain amount of stainless steel spheres with 12 mm diameter, enough to mill the carbon powder.
3. Close the container into the shaker and run the shaker for 15 minutes. This allows to grind the carbon black and make very small carbon black particles well dispersed into the solvent.
4. At the end of the previous phase, put silicone Wacker Elastosil RT 625 A/B and again IPA solvent into the container, with a proportion 1:1.
5. Close the container into the shaker and run the shaker for 15 minutes.
6. Pour the compound into the mask. Do not wait too much because the solvent, which is very volatile, will evaporate changing the viscosity quickly.
7. Pass the blade on to the mask to remove the excess of compound.
8. Wait 12 h.
9. Repeat the previous sequence of operations on a second DE substrate.
10. Bond the two DE substrates together, keeping the electrodes on the external sides.

Prescribed proportions for the different reagents have been employed, as detailed below.

3.5. Small scale sample manufacturing

In this paragraph, the steps for the preparation of small-scale DEG samples based on commercial Wacker Elastosil film and custom-prepared electrodes are illustrated. In order to evaluate the quality and reliability of the electrodes deposition procedure described so far, the procedure has been tested in the fabrication of small scale DEG samples to be used only for laboratory applications and experimental tests.

Moreover, dealing with small scale samples helped to figure out the correct laboratory equipment and spaces needed for a correct and clean fabrication procedure, which is of great importance in order to positively affect the lifetime of the final fabricated DEG.

Thus, before properly starting with the fabrication process, the following items have been set-up:

- A dedicate laboratory room with a work space in which all the manufacturing of DEG samples could be carried out, from the preparation phase to the final storage of the samples.
- All the mandatory safety equipment needed to correctly deal with silicones, CB powder, IPA and clean surfaces.
- A proper storage of the fabricated DEG samples in spaces with low humidity and ambient temperatures.

In Figure 3-7, the basic laboratory equipment used for fabrication process purpose is shown. In Figure 3-8, the operation of weighing the silicon compounds is shown.

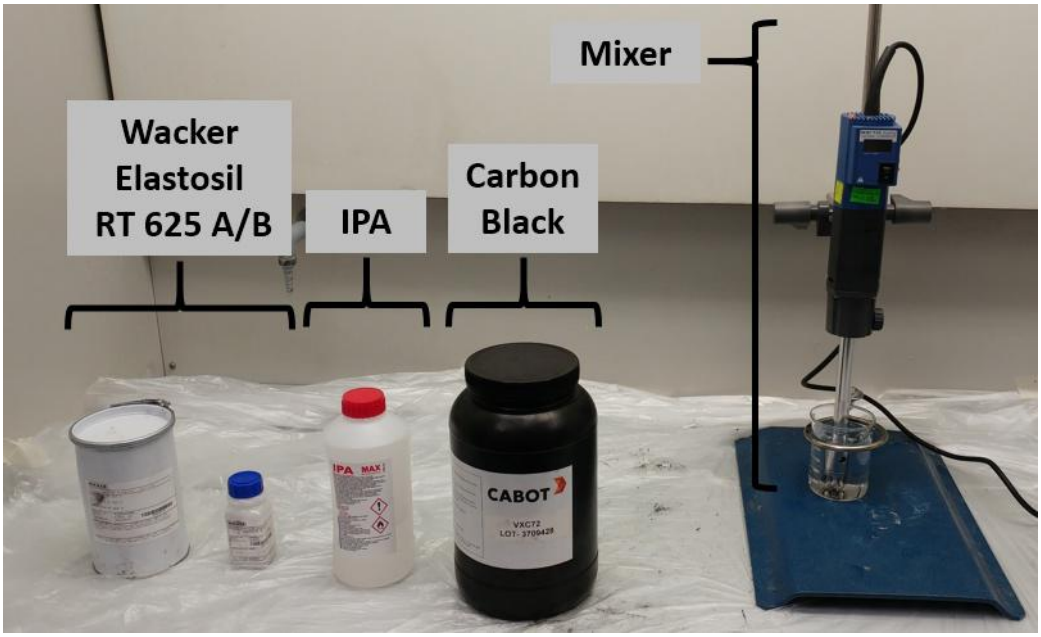

FIGURE 3-7: BASIC MATERIALS EMPLOYED FOR THE FABRICATION

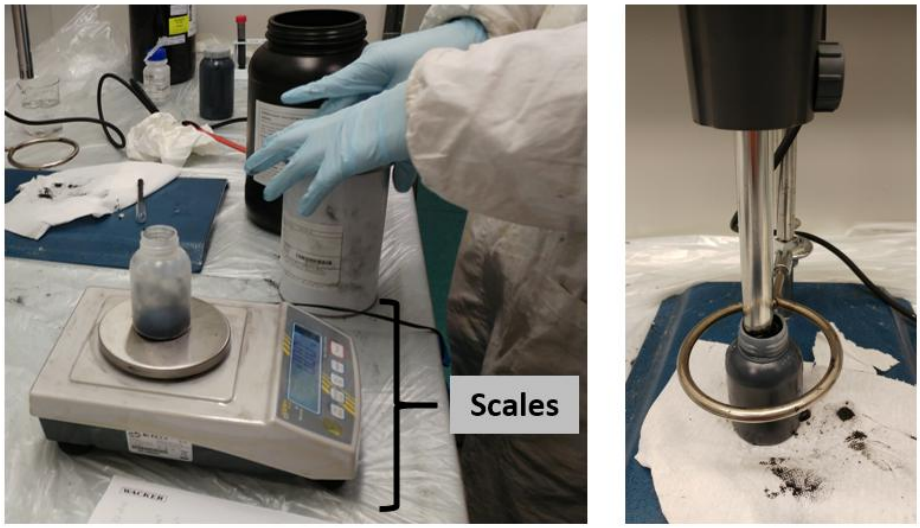

FIGURE 3-8: (LEFT) WEIGHT OUT OF COMPONENTS ON SCALES (RIGHT) MIXING OF THE COMPOUND

As already mentioned, this work mainly focuses on the fabrication process of the dielectric elastomer electrodes. Indeed, different possible recipes have been tested and refined, in order to have as result a good grade of conductivity, uniformity and deformability of the samples.

Finally, the best proportions between the electrodes components have been found to be:

- 0.8 g CB powder
- 16 g IPA: 8 g + 8 g for the two stages of the procedure
- 8 g silicone Wacker Elastosil RT 625: 7.2 g A+0.8 g B

Figure 3-9 shows an electrode sample obtained with the procedure just described and the Elastosil film used.

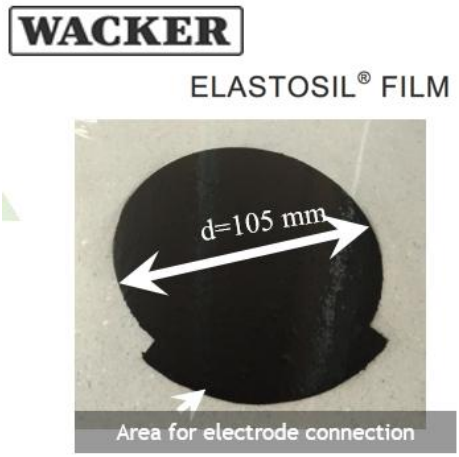

FIGURE 3-9: EXAMPLE OF SMALL SCALE ELECTRODE SAMPLE BOUNDED ON WACKER-ELASTOSIL FILM DIELECTRIC MEMBRANE

In Figure 3-10, other samples fabricated with different dimensions and electrode recipe with different support frames are illustrated.

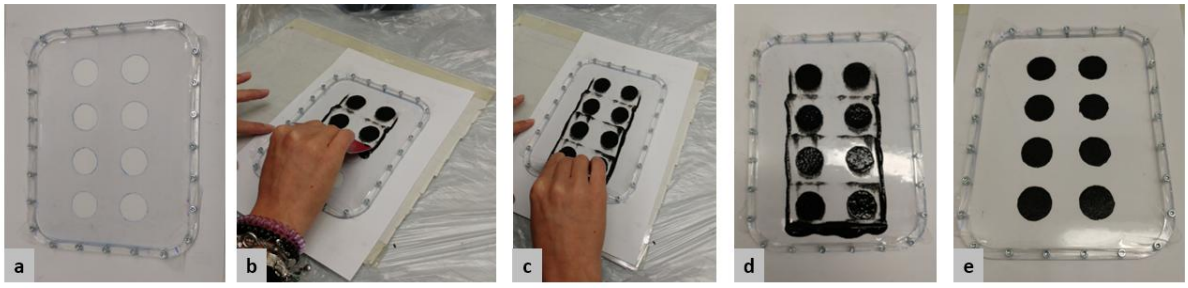

FIGURE 3-10: SMALL SCALE SAMPLES USE TO VERIFY MECHANICAL AND ELECTRICAL RELIABILITY: A – WACKER-ELASTOSIL FILM STRETCHED ON A PLEXIGLAS FRAME; B,C - CASTING THE COMPOUND ON THE ELECTRODES MASK; D - CROSS LINK WAITING TIME; E - FINAL RESULT WITHOUT THE MASK.

3.6. Scaled-up samples manufacturing

After testing the manufacturing procedure with small samples, the overall procedure has been scaled up in order to produce bigger DEG transducers, considering the correct proportions of the electrode layers recipes. As already mentioned, in the DEG-PTO manufacturing procedure both the dielectric films and the electrodes have been prepared with the same Wacker matrix, i.e. Elastosil RT 625 A/B, obtaining a reliable device whose thickness and width can be freely chosen by selecting different spacers to be added in the supports of the blade tracks. A picture of one of the manufactured intermediate-scale DEGs is shown in Figure 3-11.

The dielectric elastomeric membrane has been realized with the following procedure (see the pictures of the various steps in Figure 3-12):

1. The two silicone components, A and B, together with the solvent have been placed in the mixer and mixed for 10 min;

2. The obtained compound has been placed in a vacuum chamber and 3 vacuum cycles have been performed in order to remove the air bubbles previously incorporated;
3. The membrane thickness has been set thanks to different layers of tape (single thickness 50 μm) previously attached on the two sides of the substrate (see Figure 3-12).

Electrodes casting has been accomplished used the same procedure employed for the small-scale samples. In Figure 3-13 the casting procedure of the electrode compound is shown.

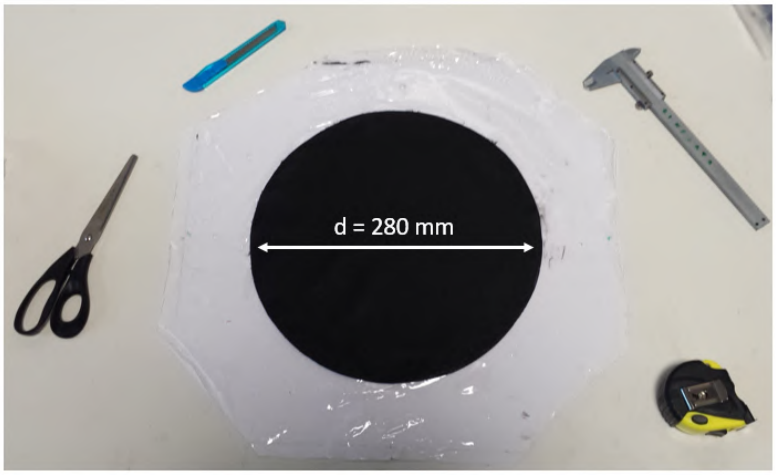

FIGURE 3-11 INTERMEDIATE SCALED DEG TRANSDUCER

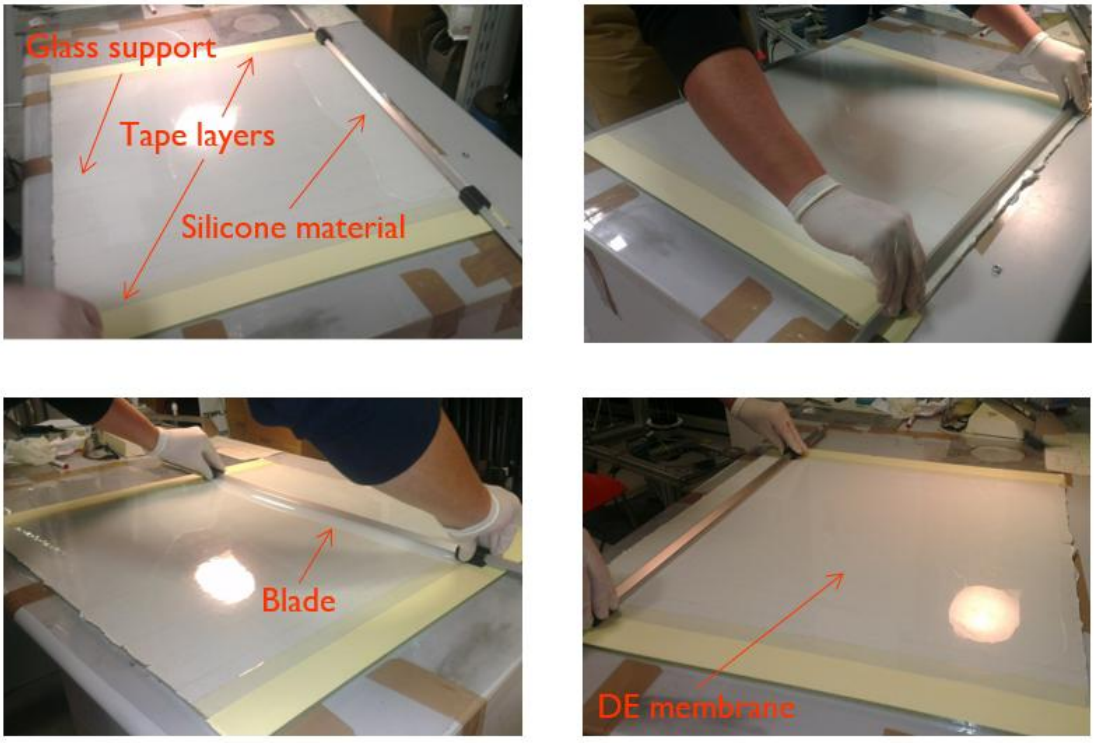

FIGURE 3-12: SEQUENCE OF OPERATION SHOWING THE CASTING PROCEDURE FOR THE DIELECTRIC LAYER

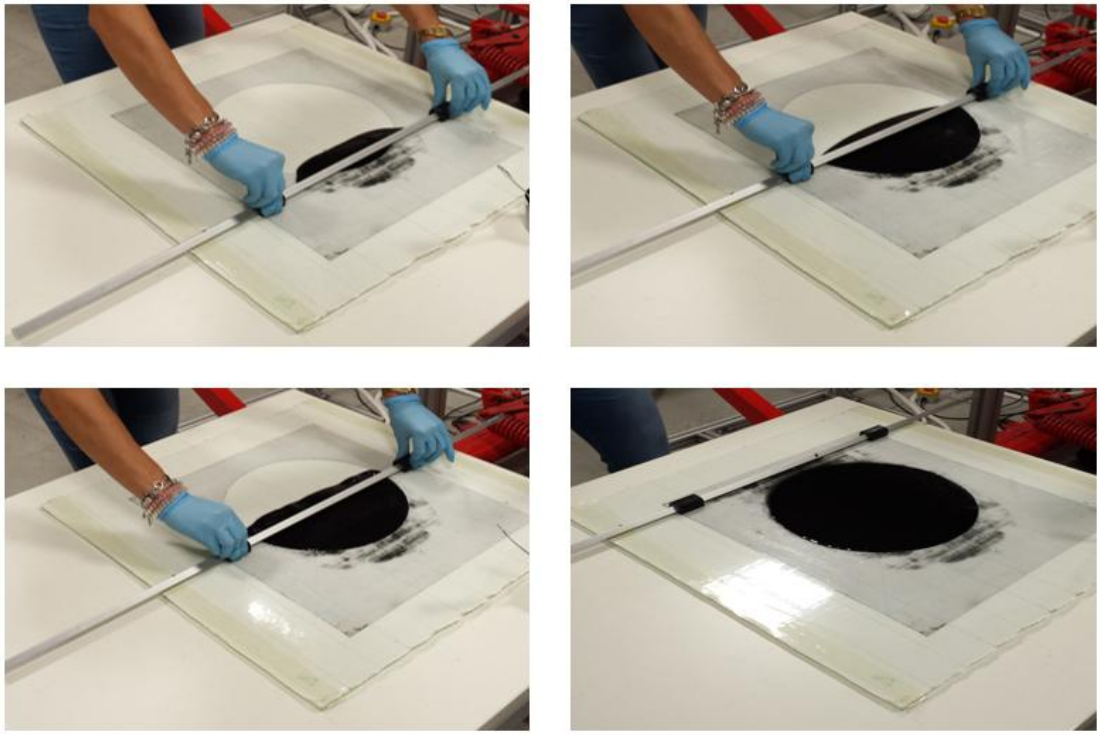

FIGURE 3-13: SEQUENCE OF OPERATION SHOWING THE CASTING PROCEDURE FOR THE ELECTRODE LAYER

As a last step, a final quality/functionality assessment test has been performed in order to determine the quality of the fabricated DEG. It consists in the measurements of the main characteristics of both the dielectric membrane, especially if custom-fabricated in the laboratory, and the electrodes.

In Figure 3-14 the LCR meter used for the electrical measurements and an example of the electrode sheet resistance measurement are presented.

FIGURE 3-14: LEFT, LCR METER MODEL HAMEG HM8118; RIGHT RESISTANCE MEASUREMENT FOR AN ELECTRODE SAMPLE

An LCR meter is an electronic test device used to measure inductance, capacitance, and resistance of an electronic component. In this application, as reported in Table 2, the sheet resistance of the electrodes and the DEG capacitance have been measured. In addition, the dielectric membrane thickness has been

measured to evaluate its dielectric constant (Equation 16), which as expected is in the good range for energy harvesting application.

$$\varepsilon_r = \frac{C\,t}{A\,\varepsilon_0}, \quad \varepsilon_0 = 8.8542 \times 10^{-12}\ \mathrm{F/m} \tag{7}$$

TABLE 2: MEASURED DEG PROPERTIES

Sample	Property	Average value	Unit	Meas. Instrument
Dielectric	Dielectric constant (ε_r)	2.86	F/m	LCR meter Micrometer
	Thickness (t)	300	μm	
	Strength	70-100	MV/m	
Electrode	Sheet resistance	350	Ω/□	

These measured properties are perfectly in line with the expected values of resistance of electrodes that are slightly exceeding the expected performance in terms of low-resistivity of the layer. This improved behavior could be attributable to the different quality of carbon-black that has been employed for the preparation of electrode mixture.

Separate tests have been conducted to verify dielectric breakdown of realized DE films. Specifically, samples like those represented in Figure 3-10 have been employed to make in-parallel testing on multiple specimens. The obtained results indicate dielectric breakdown values in the order of 70-100 MV/m, which is in line with the values of the Wacker Elastosil Film but slightly more dispersed due to the variability introduced by a manual fabrication process.

3.7. Pre-stretching and Stacking mechanism

This subsection describes the procedure that is envisaged to stack several DEG membranes, in order to electrically connect them in parallel, is described.

The stack, as shown in Figure 3-15, is obtained piling up several membranes, each one having a single electrode (e.g., on the top face). The last (bottom) membrane of the stack, differently, has electrodes casted on both sides.

Electrodes have circular shape with a number of radial strips (made of the same material as the electrode) on its perimeter. These appendages are needed to implement the connection between the compliant electrode and rigid wires of the power electronics. Radial connections on two successive electrodes (with opposite polarity) are shifted apart circumferentially in order to avoid superimpositions, thus avoids parasitic capacitance effects at the DEG perimeter.

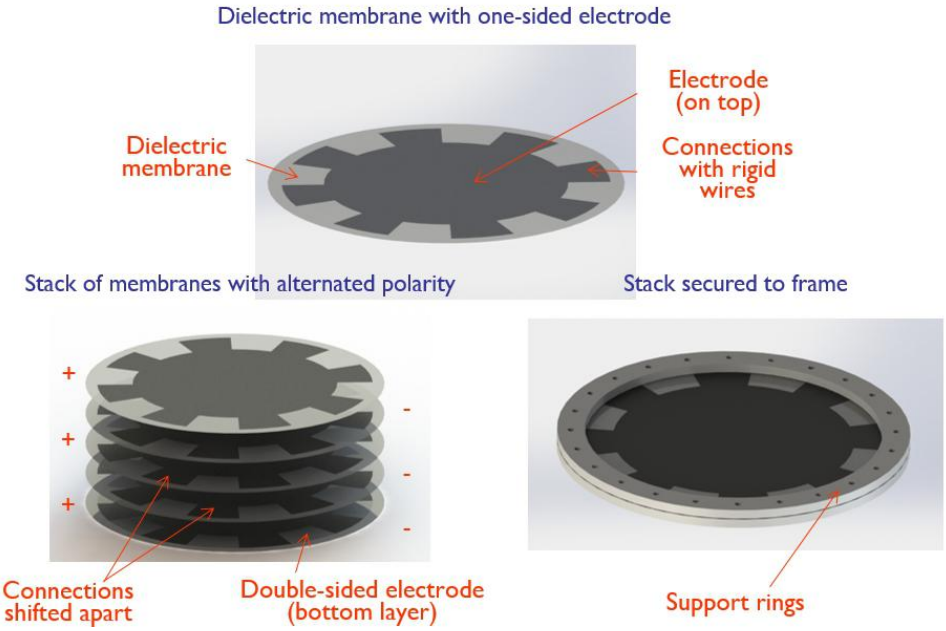

FIGURE 3-15: STACKING PROCEDURE OF A DEG ASSEMBLY

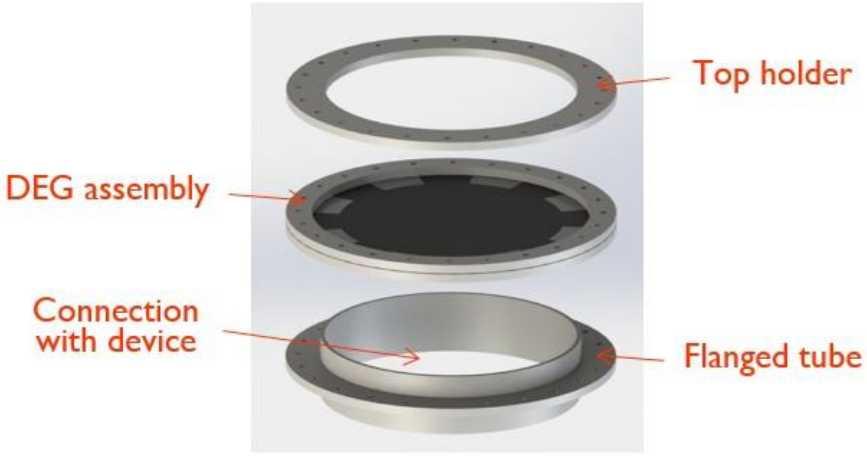

FIGURE 3-16: DEG STACK PRE-STRETCHING ON HOLDING FIXTURE

The membrane assembly is mounted on a holder made of two annular rings (see Figure 3-16) that are bolted in such a way as to squeeze the external boundary of the membrane. A flanged tube with an internal diameter equal to the inner diameter of the rings is then inserted and screwed onto the ring-holder to produce an out-of-plane deformation of the membrane and induce an equibiaxial pre-stretch in its central part (see Figure 3-17). The height of the flanged tube sets the final pre-stretch level of the assembly.

Finally, as shown in Figure 3-17, after pre-stretching, a further ring-shaped holder is bolted on the top in order to avoid slipping at the membrane perimeter. The contact with the electrodes is ensured by radial connections.

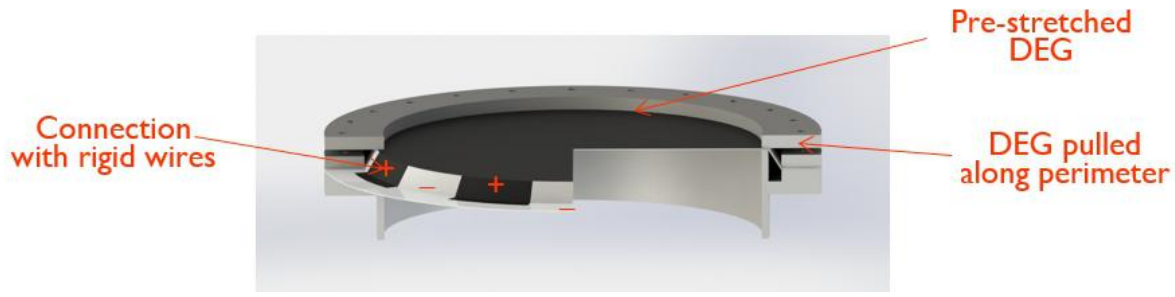

FIGURE 3-17: FINAL ASSEMBLY

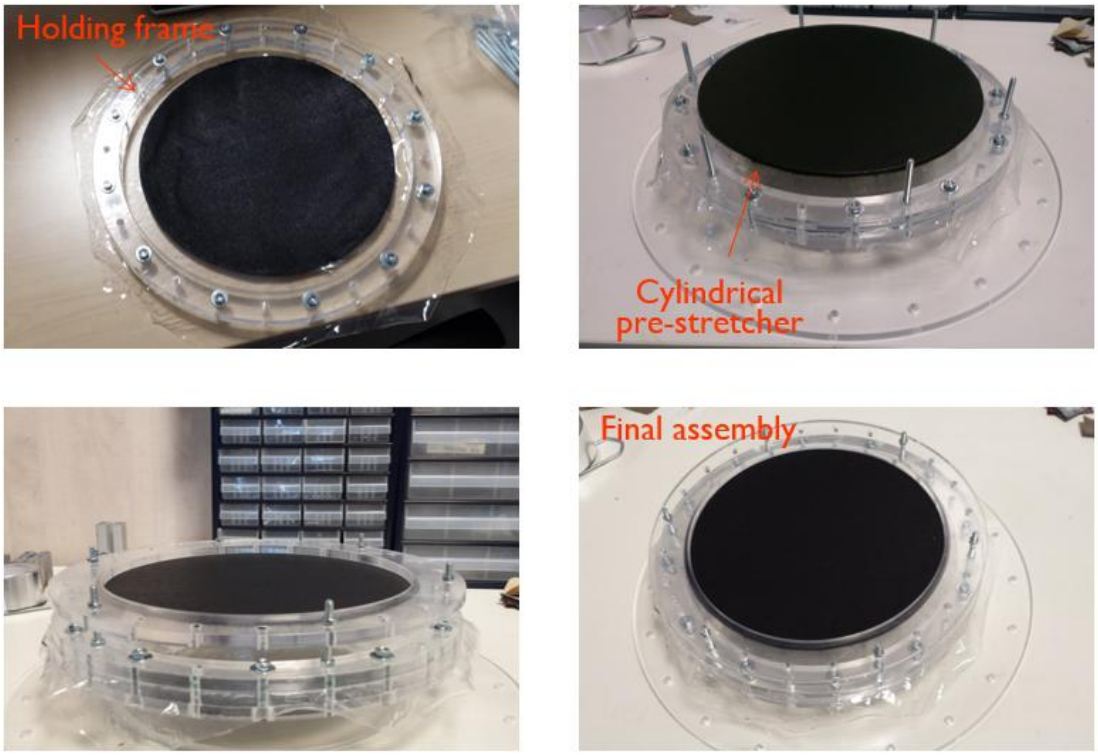

FIGURE 3-18: DEG PROTOTYPE ASSEMBLY ON THE PRE-STRETCHER

A version of the described pre-stretching mechanism has been designed and built, using custom polyacrilate parts, and it has been used to pre-stretch the scaled-up DEG membranes prototypes. The prototype is shown in Figure 3-18. Specifically, the developed collector is able to host membranes with a diameter of D=350 mm that can be held with a pre-stretch that can be regulated in a range of 1.1 to 1.3. This is the useful range that guarantee a buckling-free operation for typical silicone-based or rubber-based membrane.

For the purpose of a first demonstration, stacks with 2 DE layers and 3 electrodes have been manufactured. A total of three prototypes have been fabricated with the aim of integrating the DEG samples with the testing setup described in Sect. 2. The basic dimensions and characteristics of the DEG-prototype are presented in the following table including the expected performance in terms of maximum converted energy per cycle and maximum power (for a reference oscillating frequency).

4. Test and results

4.1. Introduction

This section reports the testing activities and the analysis of the experimental results conducted in the last period of WP 5. These test campaigns aim at validating/refining the simulation models that have been developed in the first period of the project. Additionally, the obtained results and figures of merit make it possible to confirm the promising results obtained through theoretical investigation and through previous experiments on smaller scale models.

These experimental tests employ the novel HIL test bench setup that makes it possible to test DEG-PTO systems in the power range of 2-10 W in operational conditions with simulated hydrodynamics (see details in Section 2 of this document).

A first set of tests has been dedicated to the validation of this setup, that has been conducted by simulating a system that is a replica of a DEG-PTO system that was previously employed in a wave-tank testing campaign. Specifically, the hydrodynamics of the small scale WEC employed during the wave tank experiments is replicated in simulation and an exact replica of the DEG-PTO is built in order to have nearly one-to-one correspondence of the results. By operating the system in HIL, the dynamic response and the power output of the simulated and real systems are compared.

Following these validation experiments, a prototype of the novel PTO, manufactured according to the procedure described in Section 3, is integrated and a set of tests are run in order to characterize the performance of this new system.

4.2. Validation tests

This subsection reports the first set of tests that have been conceived to validate the developed HIL test-bench (see Section 2 for more details on the HIL setup). In the first part, a brief summary of the available wave tank-test and data is presented, which were available to be compared with laboratory HIL results.

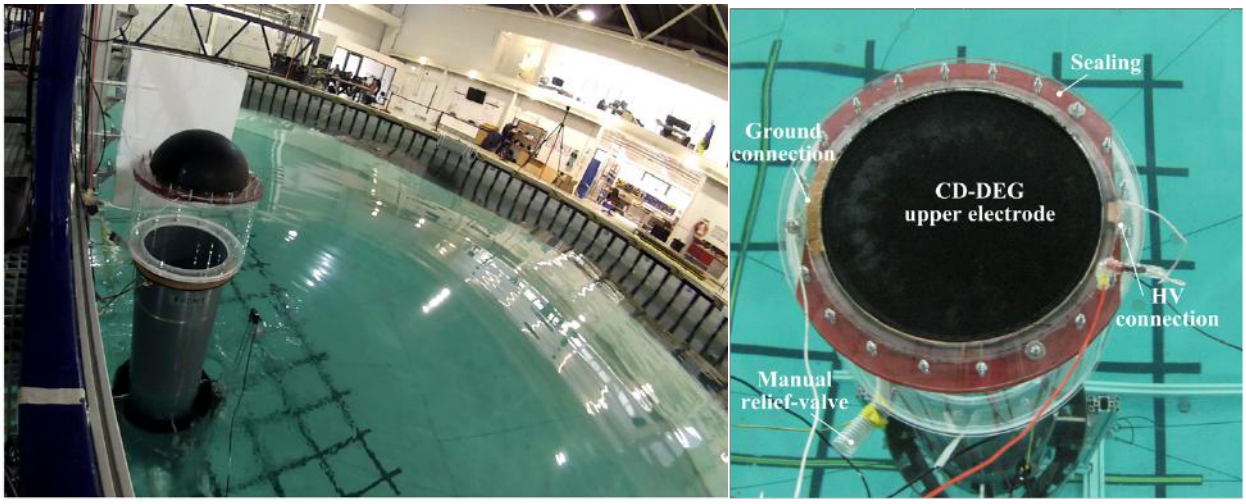

FIGURE 4-1: PICTURES OF THE EXPERIMENTAL SETUP DURING THE WAVE TANK TESTS THAT WERE PREVIOUSLY CONDUCTED BY SOME PARTNERS OF THIS PROJECT AND ARE USED FOR THE PURPOSE OF VALIDATION OF THE HIL SETUP.

In the following, a simplified linear hydrodynamic model suitable for real-time simulation of the dynamics of the WEC is presented, to be later integrated on the HIL system. A prototype of the DEG-PTO system that exactly replicates the one employed during the wave-tank tests is deployed and integrated in the HIL system. Finally, HIL tests are illustrated and results are compared with wave-tank data for validation purpose showing suitable matching.

4.2.1. Available wave-tank test results

The scheme of the small scale (approximately 1:30) WEC employed during the wave-tank test is shown in Figure 4-2(a). This is an OWC-WEC that takes the name of U-OWC, equipped with an inflatable DEG. The power scale of this device is in the order of 3-4 W which perfectly fits the power range of the HIL setup and allows a one-to-one scale reproduction of the experiments. In the following, a brief description of the system (collector and PTO) is provided.

U-OWC Collector description

The U-OWC collector (shown in Figure 4-2(a)) consists of two coaxial shells: an inner shell, which encloses the water column, and a coaxial outer shell. The cylindrical ring volume enclosed in between the two cylindrical shells act as an acceleration duct (namely, added-mass duct), which has the aim of increasing the inertia of the system, thus making it possible to tune the device with incoming waves. Moreover, the external cylinder takes the water inlet section closer to the free surface, thus increasing the excitation force of the waves on the water column. A convergent-divergent duct located inside the inner shell provides a further increase in the hydrodynamic inertia. Openings located at the bottom of the inner cylinder connect the added mass duct to the water column.

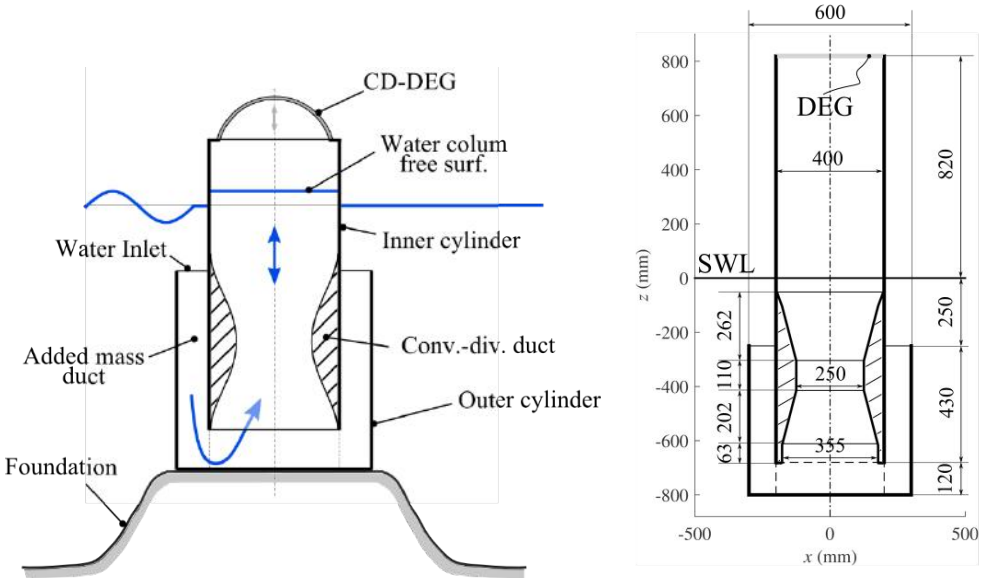

(a) **(b)**

FIGURE 4-2: (A) SCHEMATIC OF A U-OWC WITH CD-DEG. (B) LAYOUT AND DIMENSIONS (IN MM) OF THE CONSIDERED U-OWC COLLECTOR.

DEG-PTO

The system for wave-tank tests was equipped with a very simple DEG-PTO made of suboptimal materials, that however integrated all the basic functionalities to achieve effective demonstration of energy conversion form wave energy to electricity. Specifically:

- The ECU

The ECU is a double layer system composed of two dielectric layers and three electrode layers (see Figure 4-3). The high voltage electrode is the central one (protected by the two layers of dielectric) while the two external electrodes are connected to ground. The two capacitances, associated with the two layers of this ECU, are thus connected in parallel making it possible to achieve a total capacitance that is the sum of the two. The material employed for the dielectric is the acrylic rubber VHB produced by 3M. The electrodes are obtained by painting the surface of the dielectric material with a conductive grease (MG-Chemicals 846). Upon pre-stretching, each layer measures 390 mm in diameter and 0.1 mm in thickness.

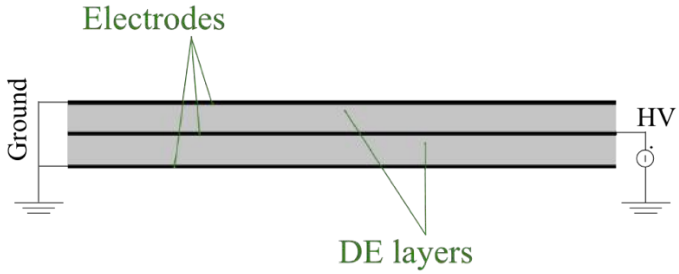

FIGURE 4-3: SCHEME OF THE DOUBLE LAYER ECU WITH GROUND ELECTRODES OUTSIDE AND HIGH VOLTAGE ELECTRODES BETWEEN THE TWO DIELECTRIC LAYERS.

- The power electronics:

The power electronic circuit is shown in Figure 4-4, and it includes: three resistors (R_1, R_2 and R_3), 3 HV switches, S_1, S_2 and S_3 (HM12-1A69-150 by MEDER electronic), and two capacitors: the ECU (with variable capacitance, C) and an in-parallel capacitor with constant capacitance C_c. A HV power supply (10/10B-HS by TREK) is used to activate the ECU at each cycle. Control of the ECU is performed based on a cyclic sequence of operations, similarly to what is described in Section 1. The ECU is kept electrically active only while its capacitance is decreasing, and the sequence of operations composing the control cycle is as follows:

1. Expansion phase. At the beginning of each cycle (while the ECU is expanding upward or downward), Cc is charged to a fixed voltage, V=0, by the power supply (during this phase, S_1 is kept closed).
2. Priming phase. When the ECU capacitance reaches a maximum, S_1 is opened, S_2 is closed, and Cc reaches an equilibrium voltage, V_a with the ECU (almost instantaneously).
3. Harvesting phase. As the ECU moves towards the flat configuration (i.e., its capacitance decreases), S_2 remains closed and the parallel Cc and C is isolated from the external supply (i.e., the total charge is constant, except for the charge losses through the DE layers).
4. Discharging phase. When the ECU membrane is flat, S_2 is opened, S_3 is closed and the ECU is fully discharged on resistor R_3. Switch S_3 is then opened and the successive cycle is started.

The use of the in-parallel capacitance, C_c, has two motivations. One the one hand, priming the CD-DEG using the in-parallel capacitor rather than directly with the power supply allows an accurate estimate of CA (the DEG capacitance at priming), which can be obtained from the measured equilibrium voltage between the DEG and Cc after priming.

Furthermore, increasing the overall capacitance of the parallel C-C_c, allows the conversion of large amounts of electrical energy while limiting the voltage rise on the CD-DEG, as suggested in [28].

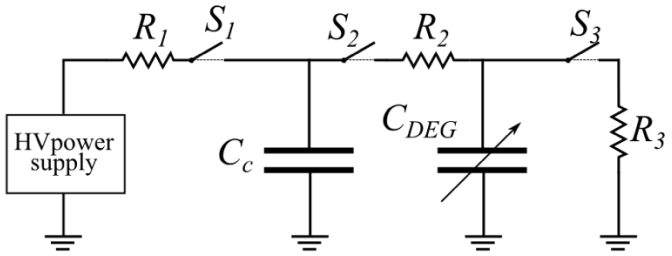

FIGURE 4-4: SCHEME OF THE ELECTRONICS EMPLOYED FOR THE DEMONSTRATION OF POWER PRODUCTION DURING THE WAVE-TANK TEST CAMPAIGN.

4.2.2. Hardware in the loop model

In order to replicate experimental conditions in HIL a real-time hydrodynamic model of a bottom-fixed axial-symmetric U-OWC device has been developed.

The geometry of the U-OWC prototype has been considered as shown in Figure 4-5, where the different dimensions are reported. Such dimensions are those of the physical prototype tested in a wave tank. A mathematical model for the collector hydrodynamics has been established and validated.

A block diagram of HIL experiments is shown in Figure 4-5. The software block of the setup takes a set of wave parameters (either regular or irregular wave parameters) as input. A software hydrodynamic model generates a wave excitation profile from the wave parameters and solves in real-time the OWC dynamic equation of motion, thus providing an output that is used to command the motion of the hardware piston. The piston displacement results in a cyclic variation of the pressure in the air chamber and a consequent deformation of the DEG.

The DEG is electrically driven by the control electronics and conditioning circuit, using the measured pressure in the air chamber as the control variable.

The control loop is closed by feeding back the measured value of the air pressure to the hydrodynamic model.

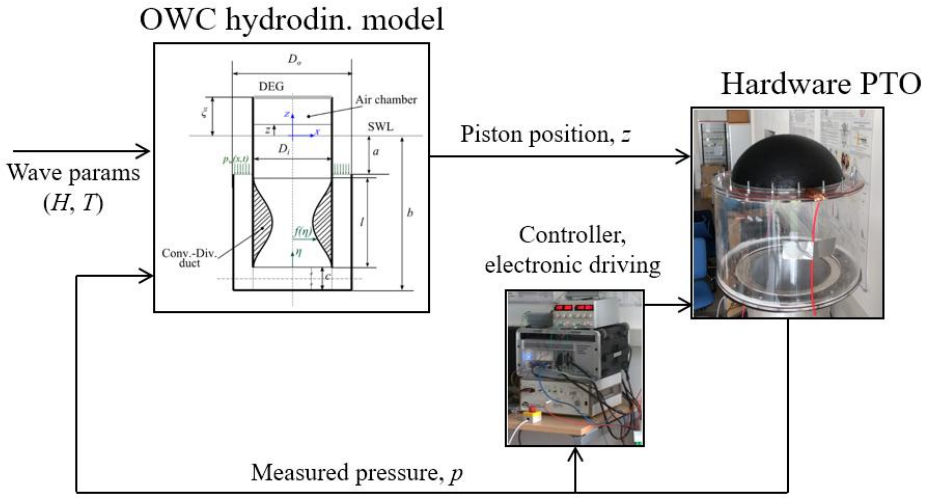

FIGURE 4-5: BLOCK DIAGRAM OF HIL TESTS

The real-time software for the hydrodynamics, electronics driving, sensors acquisition have been implemented through Matlab and Simulink scripts using the Matlab Real-time environment.

Hydrodynamic model

The fundamentals equations describing the water column dynamics are reported in the following. We make reference to the U-OWC geometry shown in Figure 4-6. We consider a reference ξ-η-ζ frame with vertical ζ axis and the origin lying on the Still Water Level (SWL). The OWC features:

- The water column, comprised within the inner cylindrical shell, whose with respect to the SWL is denoted by z. The cross-section radius of the water column is indicated with $r(\zeta)$, as it generally varies with ζ. In correspondence of the water column free surface, $\zeta = z$ and $r(\zeta)=r(z)$.
- A horizontal inlet section (with the shape of a circular ring), located at $\zeta = \zeta_i$, through which water enters/leaves the collector.
- An added mass duct, that drives water from the inlet section to the water column. The duct has outer diameter D_o and inner diameter D_i.

Water velocity in the various horizontal cross sections of the device is assumed uniform and perpendicular to the cross-sections.

The water velocity in a generic cross section of the main chamber is indicated with $v(\zeta)$ ($v(z)=\dot{z}$ at the free surface), and it is positive if the water column level is rising. The constant velocity the acceleration duct is indicated by v_i. Due to water incompressibility and mass conservation, the following equalities hold for any value of ζ:

$$\dot{m} = \rho_w \pi r^2(\zeta) v(\zeta) = \rho_w \pi (D_o^2 - D_i^2)/4 v_i = \rho_w \pi r^2(z)\dot{z} \quad (8)$$

Where ρ_w is the sea water density and $\dot{m}$ is the water mass flow through the inlet section (positive if entering the collector).

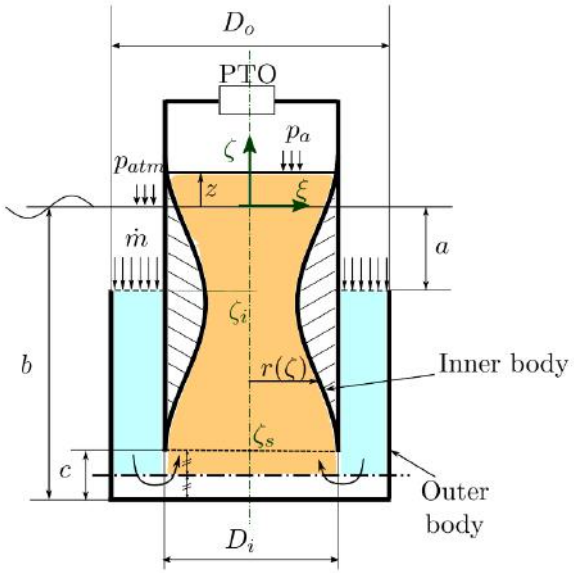

FIGURE 4-6: DEFINITION OF U-OWC DIMENSIONS AND CONTROL VOLUME

Since in the passage from acceleration duct to main chamber the water flow bends and reverts its direction, it is assumed that a stagnation volume exists at the basis of the collector, where the water can be assumed still. The stagnation surface lies at $\zeta = \zeta_s$ and, in Figure 4-6, it is marked with dash-dot line below which water is considered still. We assume that the stagnation surface lies exactly halfway along the aperture that separates the device bottom from the inner cylinder (i.e., the aperture that connects inner and outer bodies).

The device equations of motion can be derived using an energy balance approach, in the same fashion of [29][30]. Using z as coordinate, the following dynamic equation is obtained:

$$M_z(z)\ddot{z} = -C_v\dot{z}^2 - \pi\rho_w g r^2(z) z - 8\pi\rho_w K_{v,i}\frac{r^6(z)}{\left(D_o^2-D_i^2\right)^2}|\dot{z}|\dot{z} + \pi(p_e + p_r - p)r^2(z) \quad (9)$$

Where the following definitions have been introduced:

- $M_z(z)$ is the generalised inertia of the control volume (reduced to coordinate z):
- $$M_z(z) = \pi\rho_w r^4(z)\left(4\frac{b-a-c/2}{D_o^2-D_i^2} + \int_{-b+c/2}^{z}\frac{d\zeta}{r^2(\zeta)}\right) \quad (10)$$
- C_v is a quadratic term coefficient (depending on z) which accounts for z-dependent and mass advection:
  $$C_v = 2\pi\rho_w r^2(z)\left\{\left[4\frac{b-a-c/2}{D_o^2-D_i^2} + \int_{-b+c/2}^{z}\frac{d\zeta}{r^2(\zeta)}\right]r(z)r'(z) + \frac{1}{4} - \frac{4r^4(z)}{\left(D_o^2-D_i^2\right)^2}\right\} \quad (11)$$

  Where $r'(z)$ stands for the first derivative of $r(z)$.
- g is the gravity acceleration
- $K_{v,i}$ is a viscous loss coefficient, which accounts for head losses through the U-OWC collector. Its value for the collector shown in Figure 4-6 has been calibrated in and resulted in $K_{v,i}$ =6.5.
- p_e and p_r are the wave excitation pressure, and the pressure due to the radiated waves respectively [31].
- p is the air gauge pressure.

The U-OWC prototype under investigation is a point absorber, whose dimensions are much smaller than the incident wavelengths. The excitation force can be thus approximated with the Froude-Krylov

contribution only neglecting the diffraction component [32]. By fitting the expression of an undisturbed linear wave (regular wave with height H and frequency ω) [33] into equation (9), the excitation force reads as follows:

$$F_e = \pi p_e r^2(z) = \frac{\pi r^2(z)\rho_w g H}{2} \mathcal{L} \frac{\cosh(k_w(h_w - a))}{\cosh(k_w h_w)} \cos(\omega t) \quad (12)$$

Where k_w is the wave number, h_w the water depth, time is denoted by t and factor $\mathcal{L}$ comes from an integration on the inlet section and reads as follows:

$$\mathcal{L} = \frac{16}{\pi(D_o^2 - D_i^2)} \int_0^{\pi/2} \int_{D_i/2}^{D_o/2} \xi \cos(k_w \xi \cos\theta)\, d\xi\, d\theta \quad (13)$$

From this equation, an expression for the non-linear wave excitation coefficient as a function of z, is found:

$$\Gamma_z(\omega, z) = \pi r^2(z)\rho_w g \mathcal{L} \frac{\cosh(k_w(h_w - a))}{\cosh(k_w h_w)}. \quad (14)$$

Radiated wave load, $F_r = \pi r^2(z) p_r$, is more difficult to compute, as the radiation potential is a function of z and $\dot{z}$ and it is not known a priori. For this term, a linear formulation is used [34]:

$$F_r = -M_\infty \ddot{z} - \int_0^\tau k(\tau - \xi)\dot{z}(\xi) d\xi \quad (15)$$

where M_∞ is the infinite frequency-added mass. In the presented formulation, the inertia of the water column in the collector has been already kept into account through $M_z(z)$, while M_∞ is a further inertial contribution that adds up to $M_z(z)$. In the U-OWC, it is expected that the dominant inertial contribution owes to the displacement of the fluid within the collector, thus $M_z(z) \gg M_\infty$. We than assume that $M_\infty = 0$.

The convolution kernel, k, has the following well-known frequency-domain expression:

$$K(\omega) = -\omega^2(M_{ad}(\omega) - M_\infty) + i\omega B_r(\omega) \quad (16)$$

where $M_{ad}(\omega) - M_\infty$ is the frequency-dependent component of the added mass and $B_r(\omega)$ is the radiation damping.

Owing to the device axi-symmetry, the radiation damping can be computed using Haskind relation [34]:

$$B_r(\omega) = \frac{\omega k_w \Gamma_z^2(\omega, 0)}{2\rho_w g^2 \Upsilon}, \quad \text{with} \quad \Upsilon = \left[1 + \frac{2k_w h_w}{\sinh(2k_w h_w)}\right] \tanh(k h_w) \quad (17)$$

The frequency-dependent component of the added mass can be promptly computed using Kramers-Kronig relation [34]:

$$M_{ad}(\omega) - M_\infty = -\frac{2}{\pi} \int_0^\infty \frac{B_r(\xi)}{\omega^2 - \xi^2} d\xi \quad (18)$$

In numerical simulations, the convolution integral in equation (15) is approximated with a linear state-space.

The hydrodynamic model is implemented through a Simulink script which receives in input the user-defined wave parameters, the measured gauge pressure in the air chamber, and returns the command of the piston position, z_p. The piston displacement is calculated based on the simulated water column

displacement, z. At the scale of the setup, the air is approximately incompressible, thus providing a direct relationship between z_p and z:

$$z_p = \frac{1}{R_p^2}\int_0^z r^2(\zeta)d\zeta \quad (19)$$

where R_p indicates the radius of the piston.

Controller implementation

The controller implements the four-phase logics described in Sect. 2.3. Triggering between successive phases is implemented using the measured pressure signal and its derivative. The control scheme is implemented in Simulink using the Matlab RealTime simulation environment. The sampling frequency is 10 kHz.

The measured pressure is filtered via a software median filter with a span of 10 samples.

In particular, triggering between phases (1) and (2) is achieved using the value of the pressure derivative: maxima in the DEG deformation (and capacitance) are detected through the zero-crossings of the pressure derivative. A security time lag of 5 ms is waited between the aperture of switch S_1 and the closure of switch S_2. The duration of charging phase (2) is fixed, i.e., switch S_2 is kept closed for a fixed amount of time (0.2 s). To prevent DEG activation in the cycles where the membrane deformation is very small (especially in irregular waves), and generated energy would not compensate the losses, a threshold on peak pressure is set: when the pressure time-series reaches a maximum/minimum but its module is below 150 Pa, the CD-DEG is not activated.

Switching between phases (3) and (4) is based on pressure zero-crossing. Indeed, pressure becomes null when the DEG reaches the flat configuration (in correspondence of which it has minimum capacitance). A security time lag of 5 ms is waited between the aperture of switch S_2 and the closure of switch S_3. In order to avoid the inception of a quick sequence of charging and discharging phases, a minimum duration of 0.2 s is used for phase (3), regardless of the switching conditions.

The duration of phase (4) is fixed, and it is 0.2 s.

At the end of each test run, or in case of unexpected test interruption, a security switching sequence is automatically activated in order to provide complete discharge of the DEG and of the in-parallel capacitor.

4.2.3. Testing and results

This section reports on HIL testing procedures, results and performance assessment of the reference DEG prototype. A description of the sensing equipment is provided, relevant experimental time-series are reported, a procedure to estimate the electrical power generated by the DEG is described, and estimates of the electrical power outputs generated in different tests are reported.

HIL tests have been carried out using both regular and irregular wave (JONSWAP spectral distribution) simulated excitation. Each test had a first phase in which the system was tested mechanically (without electric activation), and a second phase with actual electrical control.

Relevant variables were measured as follows.

- The actual piston displacement (as opposed to the commanded piston position) was measured with the linear stage integrated encoder by Festo.
- The air chamber gauge pressure was measured with a piezo-resistive sensor (MPX12 by Freescale Semiconductor). Voltages on CD-DEG, in-parallel capacitor and power supply output were measured with custom made high-impedance (10 GΩ) probes driven by the same electronics used to control the CD-DEG.

All of the measured signals were acquired at a sampling frequency of 10 kHz.

The membrane deformed shape was monitored through a high-speed camera (Point Grey GS3-U3-23S6M-C with lens 250F6C, using acquisition software FlyCapture 2.9). Image post-processing has been carried out using computer-vision techniques that provided a set of time-series for the DEG tip elevation, *h*. The different measured signals were synchronised using analogical trigger signals.

Regular wave tests

With reference to a set of simulated regular waves (whose parameters have been fed into the numerical model of the HIL scheme) featuring the same height (H=0.2 m) and different wave frequencies, Figure 4-7 shows relevant time-series for a set of regular wave tests.

The plots show: the virtual water column elevation, z, calculated from the measured piston displacement, z_p, by inverting Eq. (19); the measured air gauge pressure, p; the membrane tip displacement, h, obtained from video frames post-processing; and the CD-DEG voltage, V. The DEG was electrically activated only during the second half of the considered time lapse. With reference to the electrically active phase, the in-parallel capacitance was $C_a = 394$ nF and the charging voltage was $V_0 = 6$ kV.

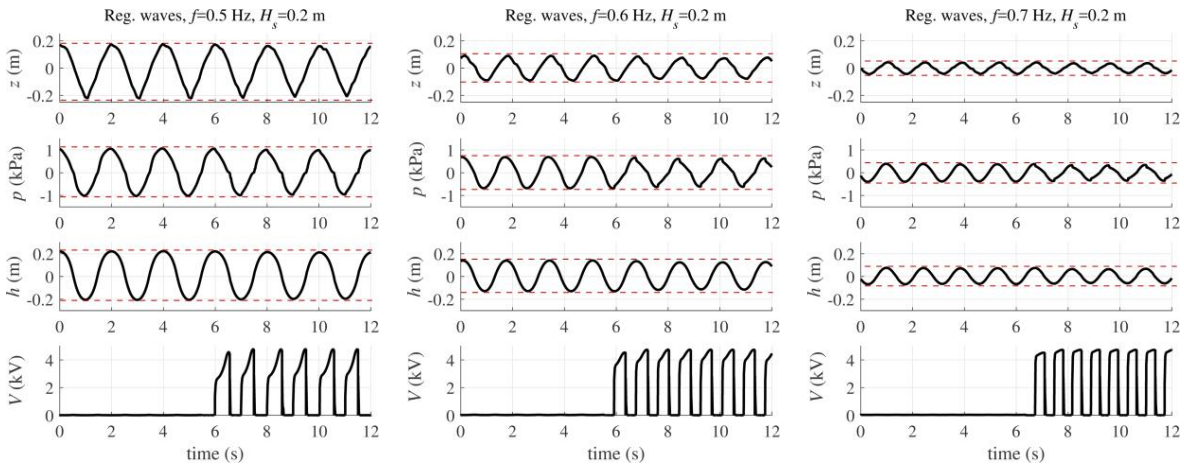

FIGURE 4-7: EXPERIMENTAL TIME-SERIES OF VIRTUAL WATER COLUMN DISPLACEMENT (Z) CALCULATED FROM THE PISTON DISPLACEMENT, AIR CHAMBER GAUGE PRESSURE (P), DEG TIP ELEVATION (H) AND CD-DEG VOLTAGE (V) FOR THREE TESTS FEATURING SAME WAVE HEIGHT (H=0.20 M) AND DIFFERENT WAVE FREQUENCIES.

A comparison of the plots shows that:

- The oscillation amplitudes are maximum at 0.5 Hz, which is indeed the natural frequency of the coupled U-OWC-DEG device under investigation, as provided by design specifications and experimentally observed in previous tests. The oscillation amplitudes decrease as the difference between excitation frequency and device natural frequency increases.

- As a result of the non-linear hydrodynamics and the measured pressure (which is influenced by the presence of the DEG), the virtual water elevation profiles are slightly asymmetric (upward vs downward oscillations), as already foreseen in previous tank tests.
- Quick electric activation provokes a jump in the air pressure. This is due to the electric-field-induced membrane expansion, that, despite small (no jump in h is indeed visible), results in a significant air pressure drop due to the high air rigidity at the experiment scale.
- The steady-state oscillation amplitudes of z, p and h in the presence of electric activation are smaller than in the first half of the experiment, in the absence of activation. The electrical control indeed damps the system dynamics, as it subtracts mechanical energy from the oscillations to transform it into electrical energy delivered to the conditioning circuit.

Although the electric setup used for electricity generation tests does not allow the delivery of the generated energy to a storage system (e.g., the generated power is dissipated through resistor R_3), an estimate of the generated electrical energy (regardless of the losses present in the conditioning circuit) is possible, based on the voltage measurements on the DEG and C_a.

The electrical energy generated by the CD-DEG in a cycle, $\mathcal{W}_u$, can be estimated as the difference between the energy harvested from the DEG and C_a during the discharging phase (3) and that spent to charge the system in phase (1) (see Sect. 2.3 for the detailed description of the phases):

$$\mathcal{W}_u = \frac{1}{2} C_B V_B^2 - \frac{1}{2} C_A V_A^2 + \frac{1}{2} C_c \, (V_B^2 - V_A^2), \qquad (20)$$

where V_A and V_B are the voltages (on the DEG and C_c) immediately after electric priming and before discharging respectively, measured by the HV probes. Capacitance C_A depends on the DEG deformation at the current cycle and is measured from charge conservation (i.e. measuring the voltage on the capacitance Cc after and before the transfer of charge) and capacitance C_B at the discharging instant is known from direct measurement on the flat DEG stack.

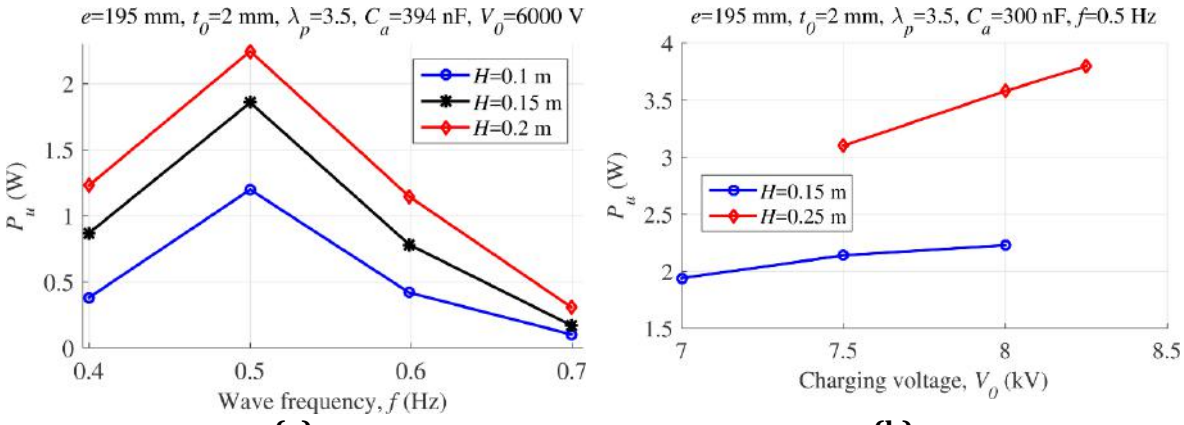

(a) **(b)**

FIGURE 4-8: EXPERIMENTAL ELECTRICAL POWER OUTPUT OF THE PROTOTYPE IN A SET OF TESTS WITH SIMULATED REGULAR WAVE EXCITATION. (A) TESTS WITH CONSTANT CHARGING VOLTAGE V_0=6 KW. (B) TESTS WITH CONSTANT WAVE FREQUENCY F=0.5 HZ (VHB PROTOTYPE).

The first term in equation (20) is the energy recovered from the DEG during discharging phase (4) The second (negative) term is the electrical energy supplied to the CD-DEG during priming (2). The third term is the energy transferred from the DEG to C_a during harvesting phase (3).

In this estimate, it has been assumed that the DEG capacitance remains constant during the discharging phase (which is almost instantaneous), i.e., voltage-induced expansion of the CD-DEG during priming is considered negligible.

With reference to the same electrical parameters (V_0 and C_a) of the data Figure 4-8.a shows the estimated power in the presence of regular wave excitation with different wave parameters (f and H). In the plot, the power is estimated from the average of $\mathcal{W}_u$ over the different cycles, and from the wave frequency, f. The first cycle after activation has been removed from the computation as it generally features different DEG oscillation amplitude with respect to the steady state response. Considering that the CD-DEG performs two generation cycles per period (one for upward and one for downward deformation), the following equality holds: $P_u = 2\mathcal{W}_u f$. The electrical power is maximum when the commanded wave frequency equals the device natural frequency (0.5 Hz) at which the oscillation amplitudes are maximum. The maximum power output in the considered set of tests is approximately 2.2 W, corresponding to 80-170kW projected to a full-scale of 20-25 times the prototype scale.

A further set of experiments was carried out, using a constant excitation frequency equal to the resonance frequency (f=0.5 Hz) and different values of the simulated wave height, H, and of the charging voltage, V_0. In such tests, an in-parallel capacitance of C_a=300 nF was used. Results, in terms of the average generated electrical power, are in Figure 4-8.b. In the plot, two different wave heights are taken into account (H=0.15 and 0.25 m). As expected, the generated power increases with increasing values of H and V_0. The increase of the generated power with V_0 is less than quadratic (although $\mathcal{W}_u$ depends quadratically on the DEG voltages throughout the cycle). This owes to two effects: (1) higher voltage results in a larger damping of the coupled OWC-DEG system, thus inducing a decrease in the maximum oscillation amplitudes of the system; (2) higher voltage results in higher electrical losses on the highly dissipative VHB layers. The latter effect is expected to have a significantly lower weight if improved DE materials are employed. A remarkable maximum power output of approximately 4 W was achieved in this set of tests. These results is in accordance with peak performance figures recorded in tank tests [35] and corresponds to almost 600 kW at full-scale.

The present results confirm those obtain through previously conducted wave tank tests, both in terms of dynamical response of the system (achievement of maximum amplitude oscillations at 0.5 Hz confirms design predictions and wave-tank observations) and of device measured power output (in the order of a few Watts).

Irregular wave tests

Irregular wave HIL tests have been performed by feeding a set of statistical wave parameters into the software hydrodynamic model and generating excitation force profiles assuming a JONSWAP spectral distribution. The following parameters have been used to generate the wave profiles: significant wave height, H_s, peak frequency, f_p, and peak enhancement factor, γ_p (a standard value of 3.3. has been used for the peak enhancement factor).

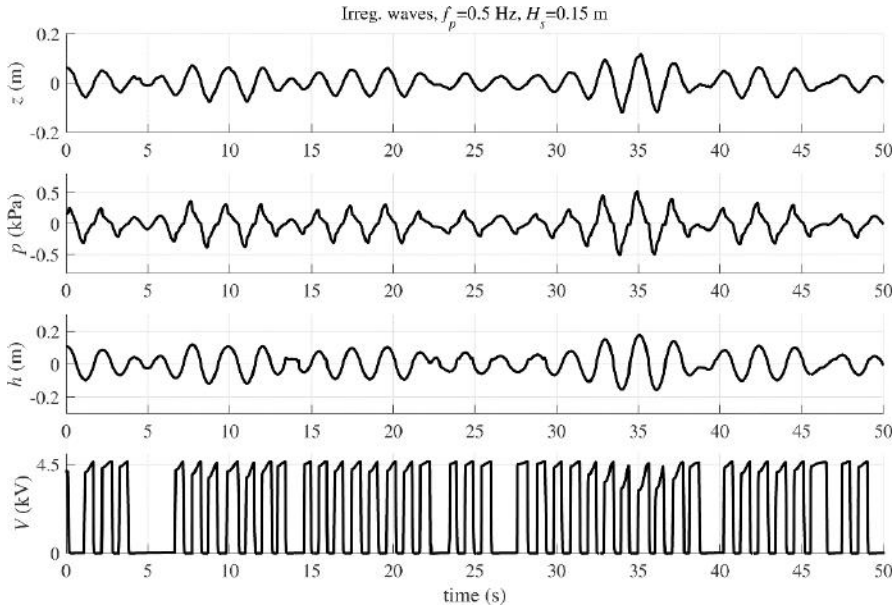

FIGURE 4-9: EXPERIMENTAL TIME-SERIES OF THE VIRTUAL WATER COLUMN DISPLACEMENT (Z) CALCULATED FROM THE PISTON DISPLACEMENT, AIR CHAMBER GAUGE PRESSURE (P), MEMBRANE TIP ELEVATION (H) AND DEG VOLTAGE (V) FOR AN IRREGULAR SEA STATE FEATURING SIGNIFICANT WAVE HEIGHT H_s=0.15 M, AND PEAK FREQUENCY f_p=0.5 HZ.

With reference to a test with H_s=0.15 m and f_p=0.5 Hz, Figure 4-9 shows the time-series of z, p, h and V in the presence of electrical control. The in-parallel capacitance is C_a=394 nF, and the charging voltage is $V_0 = 5$ kV.

The plot provides evidence of the effective operation of the CD-DEG and of its controller in irregular waves. Cyclic electric activation is effectively provided as the DEG deformation is maximum (both upward and downward deformation), and it is maintained as long as the DEG capacitance decreases (as demonstrated by the monotonically increasing voltage profiles). It is worth noticing that the control does not activate the membrane during certain cycles characterized by little membrane deformation, when the pressure module is below the threshold value of 150 Pa.

As regards power output estimate, the mean power P_u is computed as the sum of the electrical energy generated in the different cycles (calculated according to the procedure described in Sect. 2.5.2 and equation (20)) divided by the time duration of the generation test.

Figure 4-10 shows the average power output of the CD-DEG sample over a set of irregular sea states. The plot refers to a set of tests with C_a=300 nF and $V_0 = 7.5$ kV.

The power output is maximum when the peak frequency of the spectrum equals the natural frequency of the system (i.e., 0.5 Hz), although its dependence on the frequency is weaker than in monochromatic waves. A mean power of almost 1 W was successfully generated, thus proving the effective operation of the controller and of the coupled OWC-DEG system in general also in irregular waves.

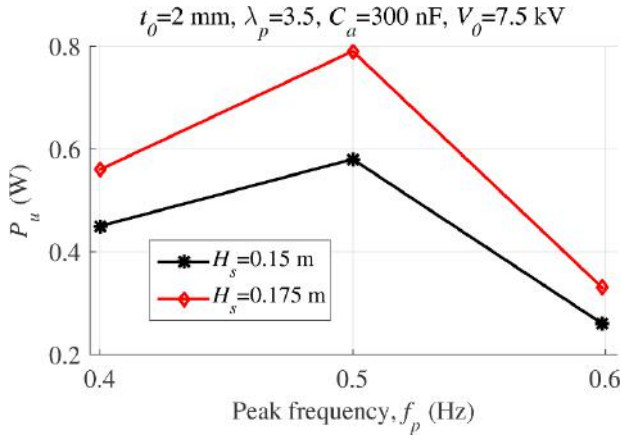

FIGURE 4-10: EXPERIMENTAL ELECTRICAL POWER OUTPUT OF THE PROTOTYPE IN A SET OF TESTS WITH SIMULATED REGULAR WAVE EXCITATION (VHB PROTOTYPE).

4.3. PDMS prototype testing

A second set of tests was carried out, combining the hydrodynamic model of the abovementioned U-OWC collector and a prototype of an advanced PDMS-based DEG, with the features shown in Table 2. Several sets of tests were carried out, using the following parameters/ranges:

- DEG diameter D=350 mm (in the flat pre-stretched configuration)
- Total undeformed thickness t_0=0.3 mm per layer including electrodes thickness. Active DE thickness: 0.25 mm approx.
- Pre-stretch λ_p =1.2
- Nr. of DE layers in parallel n_l=2
- Capacitance (in the flat pre-stretched configuration) C=70 nF

The DEG was manufactured using the procedure described in Sect. 3. In particular, a multi-layered DEG layout was achieved, based on two DE layers and three electrodes. Implementation of the multi-layered pre-stretched DEG stack was achieved as described in Sect. 3.7.

The DEG prototypes employed in these experiments featured a similar amount of DE material compared to the previous tests with VHB acrylic. However, the PDMS material employed in these experiments features larger mechanical stiffness compared to VHB. The U-OWC geometry used to build the hydrodynamic model has been purposely optimized to guarantee dynamical tuning and target power output of a few Watts in the presence of (simulated) scaled waves with a scale factor of 1:20/1:30 with respect to full-scale ocean waves. In effect, to preserve the dynamical features of the device (e.g., approximate same value of the natural frequency), the collector should be re-designed and re-optimised for operation with the new DEG PTO.
For the aim of simplicity, in the presented preliminary set of HIL tests with PDMS, no modifications in the OWC collector design were considered.
A complete set of regular wave tests has been performed, and the resulting power output in different (simulated) sea states is reported in the following. Moreover, irregular wave tests are also described.

4.3.1. Regular wave tests

With reference to a set of simulated regular waves (whose parameters have been fed into the numerical model of the HIL scheme) featuring the same height (H=0.15 m) and different wave frequencies, Figure 4-11 shows relevant time-series for a set of regular wave tests.
The plots show: the virtual water column elevation, z (calculated from the measured piston displacement, z_p); the measured air gauge pressure, p; the membrane tip displacement, h, obtained from video frames post-processing; and the CD-DEG voltage, V. The DEG was electrically activated only during the second half of the considered time lapse. With reference to the electrically active phase, the in-parallel capacitance was $C_a = 100$ nF and the charging voltage was $V_0 = 9$ kV.

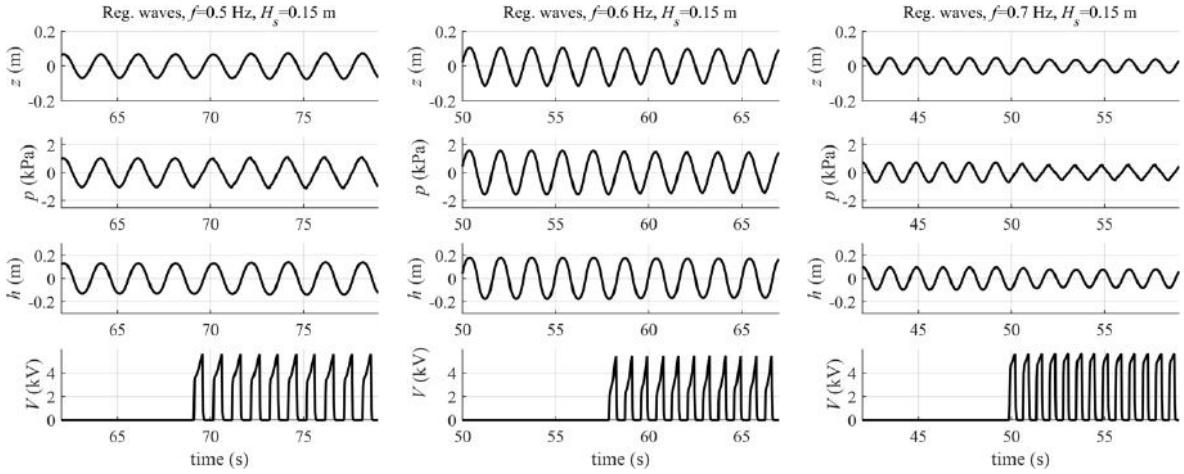

FIGURE 4-11: EXPERIMENTAL TIME-SERIES OF VIRTUAL WATER COLUMN DISPLACEMENT (Z) CALCULATED FROM THE PISTON DISPLACEMENT, AIR CHAMBER GAUGE PRESSURE (P), DEG TIP ELEVATION (H) AND CD-DEG VOLTAGE (V) FOR THREE TESTS FEATURING SAME WAVE HEIGHT (H=0.20 M) AND DIFFERENT WAVE FREQUENCIES – PDMS DEG PROTOTYPES (NEW SILICONE-BASED DEG-PTO).

Compared to the previous tests with acrylic rubber, the following can be observed:

- The natural frequency of the system, at which oscillation amplitudes are maximum, is 0.6 Hz (instead of 0.5 Hz). This is due to the larger stiffness of the PDMS DEGs, that owes to: 1) smaller DEG radius with larger thickness (in the flat pre-stretch position), 2) larger elastic modulus of the material.
- Despite the lower amplitude of the incoming waves, pressures in the air chamber (in the resonance condition) are larger, owing to the large mechanical stiffness of the DEG.
- The jump in the air pressure time-series, owing to instantaneous activation, is less prominent that in the previous tests. Owing to the larger DEG stiffness, indeed, application of a same level of electric field (in the order of tens of MV/m) results in a lower electrically-induced deformation of the DEG.
- Although at f=0.6 and 0.7 Hz the oscillation amplitudes of z, p and h in the presence of electric activation are smaller than in the first half of the experiment (due to electrical damping), at f=0.5 Hz, electrical activation induces an increase in the steady-state oscillation amplitude of the system. In this case, owing to the electric activation, the natural frequency of the device gets closer to the excitation frequency, thus compensating the increase in damping.

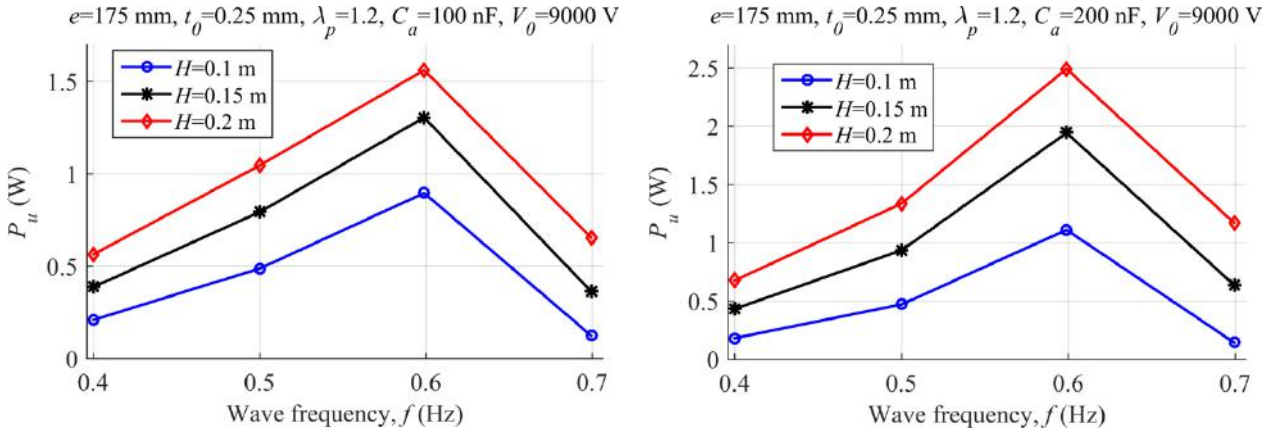

(a) (b)

FIGURE 4-12 EXPERIMENTAL ELECTRICAL POWER OUTPUT OF THE PROTOTYPE IN A SET OF TESTS WITH SIMULATED REGULAR WAVE EXCITATION WITH CHARGING VOLTAGE V_0=9 KW AND TWO DIFFERENT VALUES OF THE IN-PARALLEL CAPACITANCE: (A) C_a=100 NF, (B) C_a=200 NF (NEW SILICONE-BASED DEG-PTO).

In terms of power output performance, Figure 4-12 shows the complete prospect of the prototype measured power output in different regular wave sea states. In the plots, a charging voltage $V_0 = 9$ kV was used, with two different values of the in-parallel capacitance, namely, $C_a = 100$ nF (Figure 4-12(a)) and $C_a = 200$ nF (Figure 4-12(b)).

As in the previous case with VHB DEG, the electrical power is maximum when the commanded wave frequency equals the device natural frequency (in this case, 0.6 Hz) at which the oscillation amplitudes are maximum.

As expected, tests with larger in-parallel capacitance result in larger power outputs. Using a larger in-parallel capacitance (with same value of V_0) indeed results in larger voltages on the DEG. The maximum power output in the considered set of tests is approximately 1.6 W (with $C_a = 100$ nF), and 2.5 W (with $C_a = 100$ nF) corresponding to remarkable peak powers of up to 200-370 kW projected to a full-scale of 20-25 times the prototype scale.

Compared to previous tests with VHB DEGs, the following can be observed:

- Maximum power is reached at higher frequency than in the previous case, i.e., the device resonates in the presence of incident waves carrying a lower amount of power compared to the previous case.
- The employed amount of active DE material is slightly lower than in the previous tests (17 g of estimated dielectric material, electrodes excluded, against 20 g of VHB).
- Owing to the larger DEG stiffness, the maximum deformation reached by the DEG throughout the different sea states is, in average, slightly lower.
- Despite the last two mentioned aspects, the maximum power output achieved with PDMS is close to that achieved with VHB, meaning that PDMS enables larger convertible energy densities due to larger electrical break-down, buckling-free operation, lower viscoelastic and dielectric losses.

Further improvement in the device performance, in terms of maximum power output, might be obtained by adjusting the U-OWC collector design and adapting its dimensions to operation with PDMS prototypes.

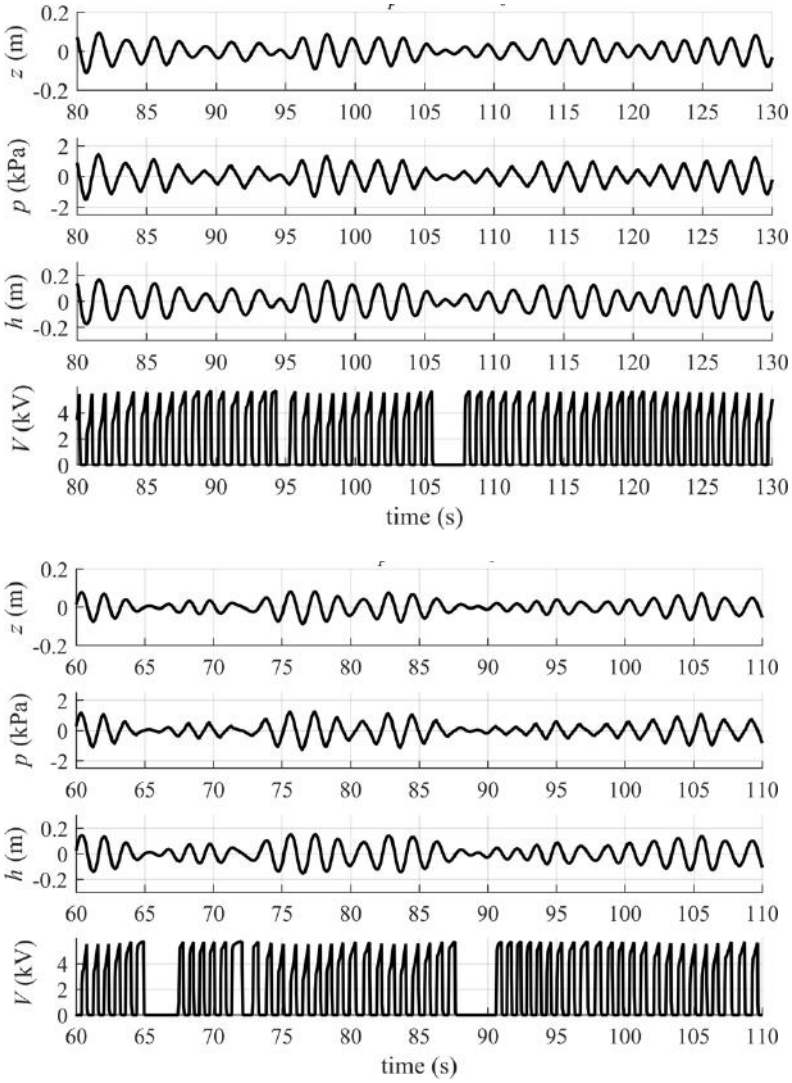

FIGURE 4-13. EXPERIMENTAL TIME-SERIES OF THE VIRTUAL WATER COLUMN DISPLACEMENT (Z) CALCULATED FROM THE PISTON DISPLACEMENT, AIR CHAMBER GAUGE PRESSURE (P), MEMBRANE TIP ELEVATION (H) AND DEG VOLTAGE (V) FOR A COUPLE OF IRREGULAR SEA STATES: A) H_s=0.15 M, f_p=0.5 HZ; B) H_s=0.175 M, f_p=0.6-PDMS DEG PROTOTYPES

4.3.1. Irregular wave tests

Similarly to the described regular wave test, a complete characterisation of the prototype response in irregular waves has been carried out. Irregular wave tests have been carried out generating irregular wave excitation profiles according to a JONSWAP spectral distribution, using a standard peakedness enhancement factor of 3.3.

With reference to a test with same DEG and same electrical layout (C_a=100 nF and V_0 = 9 kV) of monochromatic tests described in Figure 4-11 and Figure 4-12(a), Figure 4-13 shows the time-series of z, p, h and V in the presence of electrical control. The power output in the two tests is 0.52 and 0.62 W respectively. Projected to full-scale (in the hypothesis of a 1:25/1:30 scale), those values correspond to average steady-state power outputs in real seas of up to several tens of kilowatts. These are promising results, considering the simple control employed in these tests and the margin of improvement that can be achieved by refining the manufacturing process of the DEGs (migrating from a laboratory-scale

manufacturing process to a highly repeatable and accurate industrial manufacturing). Optimised DEG manufacturing is expected to allow the employment of larger electric fields (owing to the expected increase in the break-down electric field of the DE films and a reduction in the dielectric and electrodes losses).

The plots confirm the effectiveness of the device operation in irregular waves, even in the presence of the PDMS DEG PTO. As in the previous tests with VHB acrylic, the control does not activate the membrane during certain cycles characterized by little membrane deformation, when the pressure module is below the threshold value of 250 Pa (a larger value for the pressure threshold has been used compared to the previous tests with acrylic, owing to the larger stiffness of the PDMS samples).

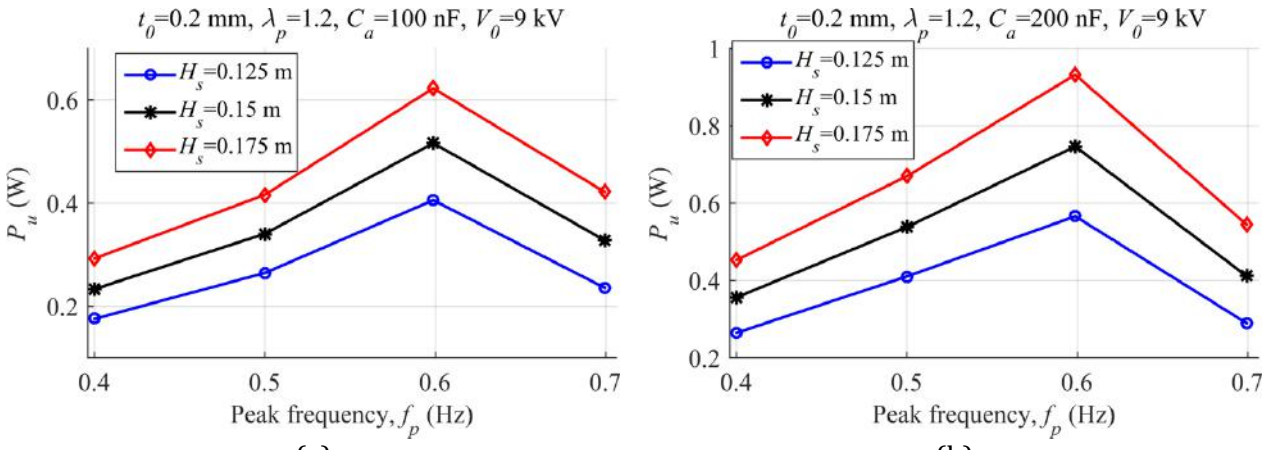

(a) (b)

FIGURE 4-14. EXPERIMENTAL ELECTRICAL POWER OUTPUT OF THE PROTOTYPE IN A SET OF TESTS WITH SIMULATED IRREGULAR WAVE EXCITATION WITH CHARGING VOLTAGE V_0=9 KW AND TWO DIFFERENT VALUES OF THE IN-PARALLEL CAPACITANCE: (A) C_a=100 NF, (B) C_a=200 NF - PDMS DEG PROTOTYPES

The trend of the prototype average power output (throughout the electrically active portion of each test) as a function of the spectral wave parameters (significant wave height, H_s, and peak period, T_p) are shown in Figure 4-14. The two plots refer to DEGs electrical driving with same charging voltage (V_0 = 9 kV) and two different values of the in-parallel capacitance (C_a=100 nF and C_a=200 nF), similarly to the presented regular wave results. The results show that the device power output is maximum when the peak period equals the natural period of the system (i.e., T_p=1.67 s), and it increases with increasing significant wave heights.

In conclusion, a comparison between results obtained with VHB acrylic and PDMS samples revealed that

- Despite the hydrodynamic interface used for the present HIL tests was specifically designed for previous tank-tests with VHB, comparable results in terms of power outputs can be achieved with PDMS samples. In general, PDMS DEGs feature larger mechanical stiffness, which results in a larger required added mass for the prototype in order to achieve resonance at a target frequency.
- Despite the rather preliminary manufacturing process employed, PDMS samples showed better performance in terms of viscous and dielectric losses compared to VHB. Indeed, similar power outputs were obtained (using similar electric field values and in the presence of same sea states), using PDMS samples with slightly lower mass compared to acrylic samples.
- PDMS samples showed a much more repeatable performance and better robustness. Differently from VHB samples, which tend to exhibit sudden and unpredictable break-down/ mechanical rupture upon repeated electrical/mechanical loading, PDMS samples show much better tolerance to cyclic

stress, and they represent a much more reliable solution for future larger-scale implementation of DEG PTOs.

4.4. Power electronics testing

This section reports preliminary results of a set of tests conducted on the power electronic module (described in Section 2 of this document) that has been designed and manufactured within the WP5 activities. Tests have been conducted on one module of the DC-DC power converter with the setup that is schematically represented in Figure 4-15.

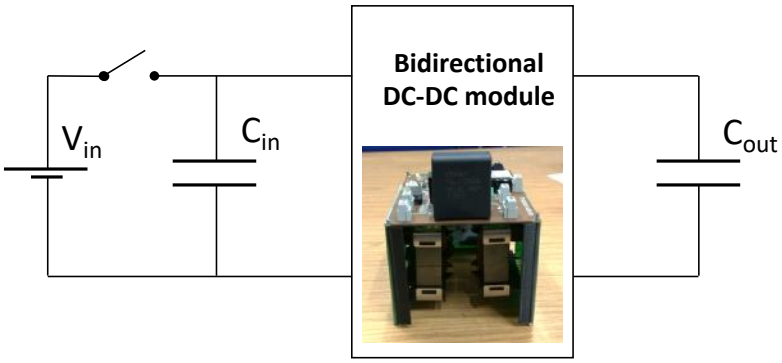

FIGURE 4-15. SCHEME OF THE EXPERIMENTAL SETUP EMPLOYED TO CHARACTERIZE THE EFFICIENCY OF THE POWER DC-DC ELECTRONICS.

μμμμconverter is employed to charge a known high voltage capacitor of C_{out}=1 μF using as power source a large capacitor C_{in}=50 μF that is initially charged through an external DC source (Trek 10-10) which is then disconnected from the system through a relay. This setup makes it possible to isolate the capacitors and the electronics allowing to accurately estimate the efficiency of this DC-DC module. The results of the tests are reported in Figure 4-16 in which measured efficiency is plotted against different initial voltages (V_{in}). The input voltage is chosen in the range of 500-900 V that corresponds to the possible working voltages across one single module of the DC-DC power system, i.e. 5-9 kV across a ten-modules system. The maximum commanded current is 50 mA and the corresponding charge time of the output capacitor is in the range of 10-20 ms. As explained in Deliverable 3.1, the charging time should be fast enough to guarantee an efficient control of DEG-PTO. In the simulations reported in deliverable D5.2 we identify that a charging time of approximately one tenth of the typical wave period could guarantee a minimum loss in the performance with reasonable requirements for the DC-DC driver. Since the developed DEG-PTO prototype is scaled down of a factor 1:20 - 1:30 and considering 10 s as a typical period time for waves, the typical scaled wave periods are in the range of 1.8-2.5 s. Thus, in the demonstrated tests, charging is roughly ten times faster with respect to the minimum requirements.

As it can be notice, the obtained efficiency spans the range of 80-90 % and it decreases as the input voltage is increased. These values are already quite promising and the margin of improvement is still broad.

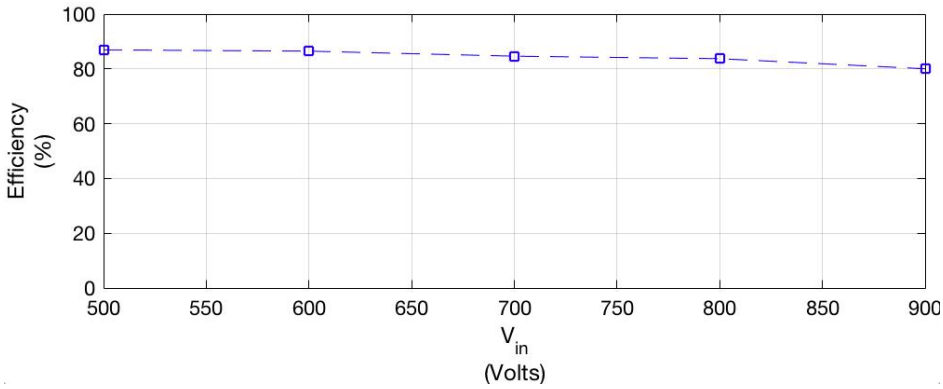

FIGURE 4-16. POWER TRANSFER EFFICIENCY VS INITIAL VOLTAGE.

Specifically, further improved results can be obtained with more advanced control strategies for the current/power transfer. The implemented current control is in fact a suboptimal method for the control of the energy that is transferred bi-directionally from one DC source to another. This constant-current charging profile has been chosen as it provides sufficient quality of the results in terms of performance at a cost of a reduced effort for its implementation.

More advanced control techniques could be implemented following for example the comprehensive approach described in [36]. The employment of such sophisticated techniques potentially makes it possible to reach values of efficiency of up to 95-97% [5]. For example, constant power control could be implemented introducing a custom firmware for the PWM management of the microcontroller. This is possible substituting the micro-controller with a more advanced controller or implementing new PWM logics on the existing microcontroller. However, these first promising results are considered sufficient for the purpose of a first demonstration. A further improved power electronics is foreseen to be designed and built in the future, in order to be integrated with an up-scaled prototype of the PTO in the range of 1-10 kW. It is worth mentioning that most of the design work conducted in this project could be employed to implement the up-scaled version of this electronics.

5. Conclusions

Conclusions

In this document, we have presented the work conducted in the framework of WP5 in the last period of the project. The activities are here focussed on the finalization of the development of a set of strategic components for the advancement of the technology of Dielectric Elastomer Generators (DEGs) for Wave Energy Converters (WECs).

Main achievements
The main achievements can be summarized as follows:

- Successful definition and implementation of a **manufacturing process** for the production of a realistic prototype of DEG based on silicone rubbers: the developed prototype is manufactured according to up-scalable techniques of shadow masking of electrodes on commercially available layers of dielectric or on custom developed dielectric elastomer layers. The fabrication procedure has been tested first at small-scale in order to verify the effectiveness of the process. The fabricated DEG-PTO is based on a commercial material developed by Wacker polymers that has been purposely conceived for dielectric elastomer generators, and it has been equipped with custom-made polymeric compliant electrodes. The developed prototype has been tested showing suitable (as foreseen) results in terms of energy density and efficiency.
  The tested production technique makes it also possible to demonstrate the feasibility of a 350 mm large multilayer prototype that features custom made DE layers and conductive electrodes. This novel prototype features improved reliability, is easier to handle and possesses high performances in terms of deformability and dielectric strength.
- **Implementation/operation and validation of a novel setup** to test DEG-PTO at 1-5 W scale: A novel custom setup that is able to run hydrodynamic simulations and drive the PTO-DEG accordingly has been developed. The system dynamic response was first validated against a set of wave-tank experiments conducted in a previous project. To this aim, a simulated hydrodynamic of the same WEC employed in the experiments has been created in order to feedback signals to the real-model of the PTO. This system makes it possible to test different types of DEG-PTOs coupled with different WEC hydrodynamics.
- **Demonstration of the operation of the DEG prototype in Hardware in the Loop (HIL) testing:** The HIL has been employed to test a new prototype of the DEG-PTO. The prototype has been realized with custom DE layers and custom electrodes. The tests were conducted in a quite safe range of electrical and mechanical loads to ensure failure-free operation. This required to recreate the real-time dynamic model of the experimental set up. Such safety margin has its negative incidence on the energetic performance of the system. Nevertheless, the obtained results are quite promising thanks to the better stability of the employed silicone membranes and to their reduced conductivity. This made it possible to reach energy density of up to 100 J/kg, i.e. values that are inline with the most performing materials. Power electronics has been studied and a fully functional module has been developed and tested.
- **Demonstration of a preliminary prototype of a bidirectional DC-DC power electronics to drive scaled DEG-PTO.**
  A first prototype of a Dual Active Bridge DC-DC converter has been designed, built and tested on a test bench in order to evaluate its actual efficiency. Results of tests conducted in in operation al condition shows that a maximum efficiency of 80-90% could be obtained with rather simplified

sub-optimal controllers. A large margin of improvement is still available; efficiency of up to 95-97% could be obtained by introducing modifications in the developed controller/ firmware.

Future works

In WETFEET project, several progresses toward the development of a full-scale prototype of WEC based on DEG-PTO have been obtained (see section "Achievements"). However, there are still several aspects that should be investigated/developed in order go further. Specifically, the following activities are currently on-going in the laboratories of some of the partners of the WETFEET consortium:

- Upscaling of the manufacturing process: study and design of a large-scale process that is based on the results obtained in this work (see Section 2) that makes it possible to manufacture DEG membranes in the range of 5-8 m in diameter.
- Fatigue and long-term response of DEG-PTO: deployment of a campaign that aims at clearly identifying the performance of the DEG-PTO in long term operational conditions. Preliminary tests have been concluded with promising results but the experiments are still to be completed.
- Design of the full scale system and study of installation/maintenance: FEED study of the integrated large scale DEG-PTO have to be conducted in order to define detailed design and to further detail the operation of installation and maintenance.
- Development of a full-scale power electronics: a prototype of a full scale power electronic system should be developed in order to efficiently drive the full scale system.

6. BIBLIOGRAPHY

[1] G. Pietro Rosati Papini, G. Moretti, R. Vertechy, and M. Fontana, "Control of an oscillating water column wave energy converter based on dielectric elastomer generator," *Nonlinear Dyn.*, vol. 92, no. 2, pp. 181–202, Apr. 2018.

[2] R. Vertechy, M. Fontana, G. P. Rosati Papini, and D. Forehand, "In-tank tests of a dielectric elastomer generator for wave energy harvesting," 2014, vol. 9056, p. 90561G.

[3] M. Righi, R. Vertechy, and M. Fontana, "Experimental Characterization of a Circular Diaphragm Dielectric Elastomer Generator," in *Proceedings of the ASME 2014 Conference on Smart Materials, Adaptive Structures and Intelligent Systems. SMASIS14*, 2014.

[4] G. Moretti, G. P. Rosati Papini, M. Righi, D. Forehand, D. ; Ingram, R. Vertechy, and M. Fontana, "Resonant wave energy harvester based on dielectric elastomer generator," *Smart Mater. Struct.*, vol. To appear, 2018.

[5] T. Todorcevic, R. van Kessel, P. Bauer, and J. A. Ferreira, "A Modulation Strategy for Wide Voltage Output in DAB-Based DC–DC Modular Multilevel Converter for DEAP Wave Energy Conversion," *IEEE J. Emerg. Sel. Top. Power Electron.*, vol. 3, no. 4, pp. 1171–1181, Dec. 2015.

[6] F. Krismer, "Modeling and Optimization of Bidirectional Dual Active Bridge DC–DC Converter Topologies," ETH Zurich, 2010.

[7] S. J. A. Koh, C. Keplinger, T. Li, S. Bauer, and Z. Suo, "Dielectric Elastomer Generators: How Much Energy Can Be Converted?," *IEEE/ASME Trans. Mechatronics*, vol. 16, no. 1, pp. 33–41, Feb. 2011.

[8] R. Pelrine, R. Kornbluh, J. Eckerle, P. Jeuck, S. Oh, Q. Pei, and S. Stanford, "Dielectric elastomers: Generator mode fundamentals and applications," *Proc. SPIE 4329, Smart Struct. Mater.*, vol. 42, pp. 148–156, 2001.

[9] A. Motaghi, A. Hrymak, and G. H. Motlagh, "Electrical conductivity and percolation threshold of hybrid carbon/polymer composites," *J. Appl. Polym. Sci.*, vol. 132, no. 13, p. n/a–n/a, Apr. 2015.

[10] G. Kofod, P. Sommer-Larsen, F. Carpi, R. K. Danilo De Rossi, R. Pelrine, and P. S. Larsen, "Compliant electrodes: solutions, materials and technologies," in *Dielectric Elastomers as Electromechanical Transducers*, 2011, pp. 69–76.

[11] S. Rosset and H. R. Shea, "Flexible and stretchable electrodes for dielectric elastomer actuators," *Appl. Phys. A*, vol. 110, no. 2, pp. 281–307, Feb. 2013.

[12] H. F. Schlaak, M. Jungmann, M. Matysek, and P. Lotz, "Novel multilayer electrostatic solid state actuators with elastic dielectric," 2005, vol. 5759, p. 121.

[13] O. A. Araromi, A. T. Conn, C. S. Ling, J. M. Rossiter, R. Vaidyanathan, and S. C. Burgess, "Spray deposited multilayered dielectric elastomer actuators," *Sensors Actuators A Phys.*, vol. 167, no. 2, pp. 459–467, Jun. 2011.

[14] G. Kofod, "Dielectric elastomer actuators," The Technical University of Denmark, 2001.

[15] A. P. Robinson, I. Minev, I. M. Graz, and S. P. Lacour, "Microstructured Silicone Substrate for Printable and Stretchable Metallic Films," *Langmuir*, vol. 27, no. 8, pp. 4279–4284, Apr. 2011.

[16] E. Tekin, B.-J. de Gans, and U. S. Schubert, "Ink-jet printing of polymers ? from single dots to thin film libraries," *J. Mater. Chem.*, vol. 14, no. 17, p. 2627, Aug. 2004.

[17] F. B. Madsen, L. Yu, P. S. Mazurek, and A. L. Skov, "A simple method for reducing inevitable dielectric loss in high-permittivity dielectric elastomers," *Smart Mater. Struct.*, vol. 25, p. 075018, 2016.

[18] T. Vu-Cong, C. Jean-Mistral, and A. Sylvestre, "Impact of the nature of the compliant electrodes on the dielectric constant of acrylic and silicone electroactive polymers," *Smart Mater. Struct.*, vol. 21, no. 10, p. 105036, Oct. 2012.

[19] S. Rosset, O. A. Araromi, S. Schlatter, and H. R. Shea, "Fabrication Process of Silicone-based Dielectric Elastomer Actuators.," *J. Vis. Exp.*, no. 108, p. e53423, Feb. 2016.

[20] D. Wang, X. Zhang, J.-W. Zha, J. Zhao, Z.-M. Dang, and G.-H. Hu, "Dielectric properties of reduced graphene oxide/polypropylene composites with ultralow percolation threshold," *Polymer (Guildf).*, vol. 54, no. 7, pp. 1916–1922, Mar. 2013.
[21] C. Ramirez, F. M. Figueiredo, P. Miranzo, P. Poza, and M. I. Osendi, "Graphene nanoplatelet/silicon nitride composites with high electrical conductivity," *Carbon N. Y.*, vol. 50, no. 10, pp. 3607–3615, Aug. 2012.
[22] E. T. Thostenson, Z. Ren, and T.-W. Chou, "Advances in the science and technology of carbon nanotubes and their composites: a review," *Compos. Sci. Technol.*, vol. 61, no. 13, pp. 1899–1912, Oct. 2001.
[23] M. H. Al-Saleh and U. Sundararaj, "A review of vapor grown carbon nanofiber/polymer conductive composites," *Carbon N. Y.*, vol. 47, no. 1, pp. 2–22, Jan. 2009.
[24] B. Li and W.-H. Zhong, "Review on polymer/graphite nanoplatelet nanocomposites," *J. Mater. Sci.*, vol. 46, no. 17, pp. 5595–5614, Sep. 2011.
[25] G. Berselli, R. Vertechy, G. Vassura, and V. Parenti-Castelli, "Optimal Synthesis of Conically Shaped Dielectric Elastomer Linear Actuators: Design Methodology and Experimental Validation," *IEEEASME Trans. Mechatronics*, vol. 16, no. 1, pp. 67–79, 2011.
[26] G. Moretti, M. Fontana, and R. Vertechy, "Modeling and control of lozenge-shaped dielectric elastomer generators," in *ASME 2013 Conference on Smart Materials, Adaptive Structures and Intelligent Systems*, 2013, pp. 1–10.
[27] G. Moretti, M. Righi, R. Vertechy, and M. Fontana, "Fabrication and Test of an Inflated Circular Diaphragm Dielectric Elastomer Generator Based on PDMS Rubber Composite," *Polymers (Basel).*, vol. 9, no. 12, p. 283, Jul. 2017.
[28] J. Huang, S. Shian, Z. Suo, and D. R. Clarke, "Maximizing the Energy Density of Dielectric Elastomer Generators Using Equi-Biaxial Loading," *Adv. Funct. Mater.*, vol. 23, no. 40, pp. 5056–5061, Oct. 2013.
[29] G. Malara, A. Romolo, V. Fiamma, and F. Arena, "On the modelling of water column oscillations in U-OWC energy harvesters," *Renew. Energy*, vol. 101, pp. 964–972, 2017.
[30] P. Boccotti, P. Filianoti, V. Fiamma, and F. Arena, "Caisson breakwaters embodying an OWC with a small opening-Part I: Theory," *Ocean Eng.*, vol. 34, no. 5–6, pp. 820–841, 2007.
[31] M. Alves, "Numerical simulations of point absorbers wave energy converters using frequency and time domain approaches," Universidade Técnica de Lisboa, 2012.
[32] T. H. Viuff, "Excitation Forces on Point Absorbers Exposed to High Order Non-linear Waves," *10th Ewtec 2013 Eur. Wave Tidal Energy Conf. Ser.*, 2013.
[33] M. E. McCormick, *Ocean engineering wave mechanics*. John Wiley & Sons, 1973.
[34] J. Falnes, *Ocean Waves and Oscillating Systems*. Cambridge University Press, 2002.
[35] G. Moretti, "Dielectric Elastomer Generators for Wave Energy Conversion: a Model-Based Design Approach," Scuola Superiore Sant'Anna, 2017.
[36] G. Ortiz, "High-power DC-DC converter technologies for smart grid and traction applications," ETH Zurich, 2014.